ADVANCED HEALTHCARE MATERIALS
www.advhealthmat.de

Self-Powered Implantable Medical Devices: Photovoltaic Energy Harvesting Review

*Jinwei Zhao, Rami Ghannam, Kaung Oo Htet, Yuchi Liu, Man-kay Law, Vellaisamy A. L. Roy, Bruno Michel, Muhammad Ali Imran, and Hadi Heidari**

Implantable technologies are becoming more widespread for biomedical applications that include physical identification, health diagnosis, monitoring, recording, and treatment of human physiological traits. However, energy harvesting and power generation beneath the human tissue are still a major challenge. In this regard, self-powered implantable devices that scavenge energy from the human body are attractive for long-term monitoring of human physiological traits. Thanks to advancements in material science and nanotechnology, energy harvesting techniques that rely on piezoelectricity, thermoelectricity, biofuel, and radio frequency power transfer are emerging. However, all these techniques suffer from limitations that include low power output, bulky size, or low efficiency. Photovoltaic (PV) energy conversion is one of the most promising candidates for implantable applications due to their higher-power conversion efficiencies and small footprint. Herein, the latest implantable energy harvesting technologies are surveyed. A comparison between the different state-of-the-art power harvesting methods is also provided. Finally, recommendations are provided regarding the feasibility of PV cells as an in vivo energy harvester, with an emphasis on skin penetration, fabrication, encapsulation, durability, biocompatibility, and power management.

1. Introduction

With advances in microelectronics and nanofabrication, biomedical implantable devices[1,2] now play an increasingly significant role in the diagnoses, treatment, and monitoring of various diseases using miniaturized and high-resolution biosensors,[3,4] reliable power transducers,[5,6] and efficient integrated circuitry.[2,4,7,8] A variety of subcutaneous devices such as defibrillators,[9] pacemakers,[6,10] cochlear implants,[11,12] drug pumps[13,14] as well as muscle, retinal, and neurological stimulators[15,16] are now being used for clinical applications. For instance, to avoid sudden heart failure, patients who suffer from heart diseases require long-term heart rhythm monitoring and analysis. Moreover, a defibrillating shock is administered during cardiac arrest. Such technologies work in harmony with personalized medical devices (e.g., wearables) and have great potential for real-world use.

However, power harvesting or generation is still a main challenge in such implantable devices. Most implantable devices are powered solely using batteries, which need eventual surgical replacement.[17] Some of the limitations of these devices include their size, lifespan, and the risk of batteries leaking toxic hazardous substances. Therefore, current miniaturization efforts require a reduction in the weight and size of these devices.[2] Due to the limited battery capacity, there is an urgent need for transducers to harvest power from the human body or the ambient environment to extend battery lifetime.

There are a variety of approaches for harvesting energy from the subcutaneous environment using photovoltaic (PV) cells, radio frequency (RF) harvesters, piezoelectric generators (PEGs), thermal electric generators (TEGs), biofuel cells (BC), as well as other hybrid energy harvesting techniques. **Figure 1**c shows the RF energy harvesting technique using a retinal stimulating system.[18] Unfortunately, many of these techniques have limitations due to their large size, low output power density, or unstable energy output.

In comparison with the aforementioned approaches, implantable PV cell technology converts abundant energy from the sun into useful electrical power.[19] For PV power harvesters to be effective in implantable devices, they need to deliver a steady

J. Zhao, Dr. R. Ghannam, K. O. Htet, Y. Liu, Prof. V. A. L. Roy, Prof. M. A. Imran, Dr. H. Heidari
James Watts school of Engineering
University of Glasgow
Glasgow, G12 8QQ, UK
E-mail: Hadi.Heidari@glasgow.ac.uk

Prof. M.-k. Law
State Key Laboratory of Analog and Mixed-Signal VLSI
AMSV
University of Macao
Macao, China

Dr. B. Michel
Smart System Integration
IBM Research GmbH
Rueschlikon CH-8803, Switzerland

The ORCID identification number(s) for the author(s) of this article can be found under https://doi.org/10.1002/adhm.202000779

DOI: 10.1002/adhm.202000779

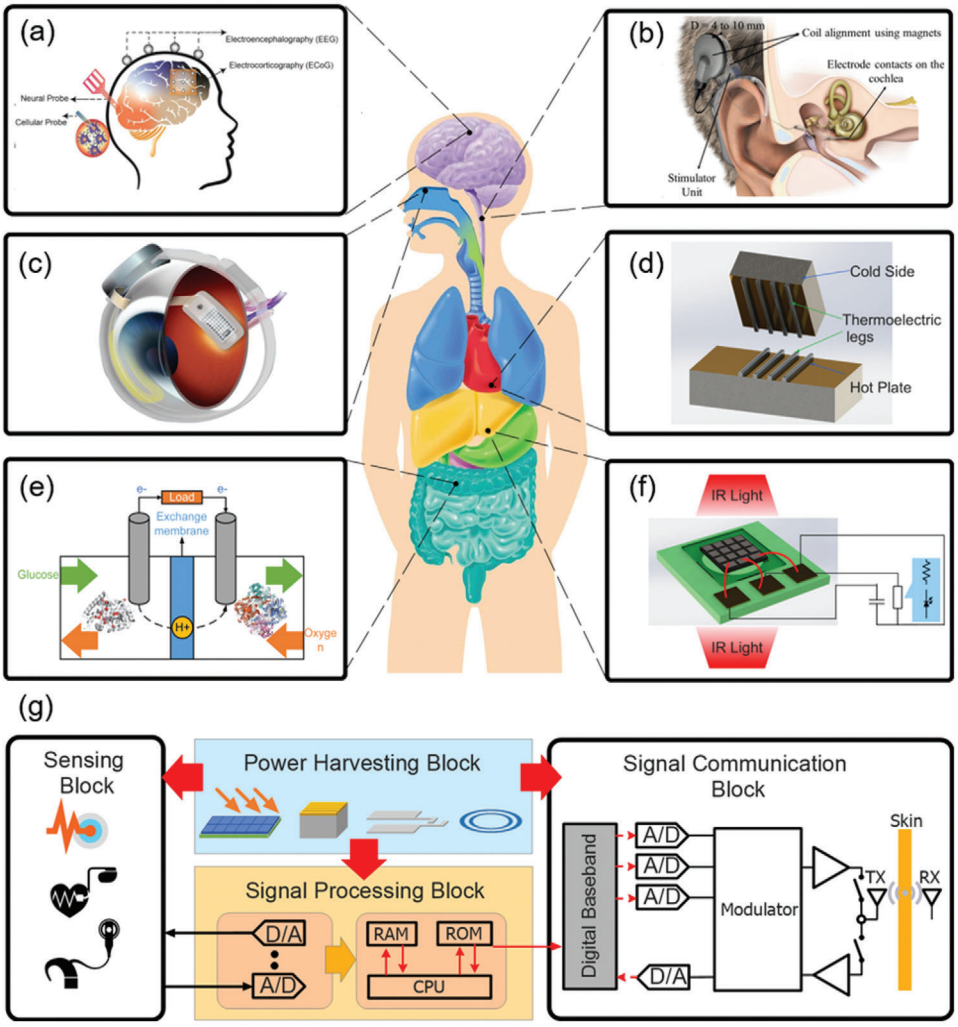

Figure 1. Implantable biomedical power harvesting applications. a) A bio-implantable system of a neurostimulator,[1] b) A ultrasonic energy harvester in usage of a cochlear hearing aid,[11] c) Retinal application powered by RF Energy harvester.[25] d) Thermal electric energy harvester in application of Cardiac implants,[25,26] e) A enzyme biofuel generator collecting power from surrounding glucose, f) PV cell in application of neuro stimulator[27] and g) The schematic diagram of the implantable applications, which contains four blocks: sensing block, power harvesting and conditioning block, signal processing block, and signal communication block.[28] Reproduced with permission.[1,18] Copyright 2020, IEEE and Copyright Clearance Center.

and high output power density. The modular nature of PV cells enables them to be configured and stacked with flexibility such that the output power and voltage of an implantable application can be met. Moreover, advanced methods have been proposed in the literature to improve the efficiency of this technology using light trapping techniques,[20,21] maximum power point tracking (MPPT),[8,22] and other power management techniques.[22–24]

Nevertheless, there are challenges in using PV cells in implantable applications, which include: 1) Rigid PV materials. Almost 90% of PV cell materials are on crystalline silicon materials, which are rigid and require expensive manufacturing techniques. To overcome these issues, emerging low-cost flexible materials are becoming a competitive candidate. However, these fabricated devices still suffer from low-grade performance and poor stability. 2) Encapsulation needs to be transmissive to improve light penetration in the PV cell, yet sufficiently protective to prevent corrosion from the internal human body. The biocompatibility and flexibility of the material used in encapsulation also requires testing to avoid the side effects of the human body and to comfort the muscles. 3) Light reaching implantable PV cells is heavily attenuated due to tissue losses, which limits the amount of harvestable energy. Consequently, an investigation into how light penetrates through different types of human tissue is required. In fact, all implantable power harvesters need to be biocompatible and sustainable for in vivo evaluation. In this case, all negative side-effects to humans should be minimized.

Thus, in this article, we provide an overview of the energy harvesting techniques that have been adopted in implantable devices. We first present the typical power requirements of various implantable devices. Next, we discuss the merits and drawbacks of each technology. In particular, our article will focus on harvesting energy from 1) light using PV cells, 2) motion using PEGs, 3) electromagnetic energy using RF harvesters, 4) heat using TEGs, and 5) biochemical energy using BC. We will demonstrate how

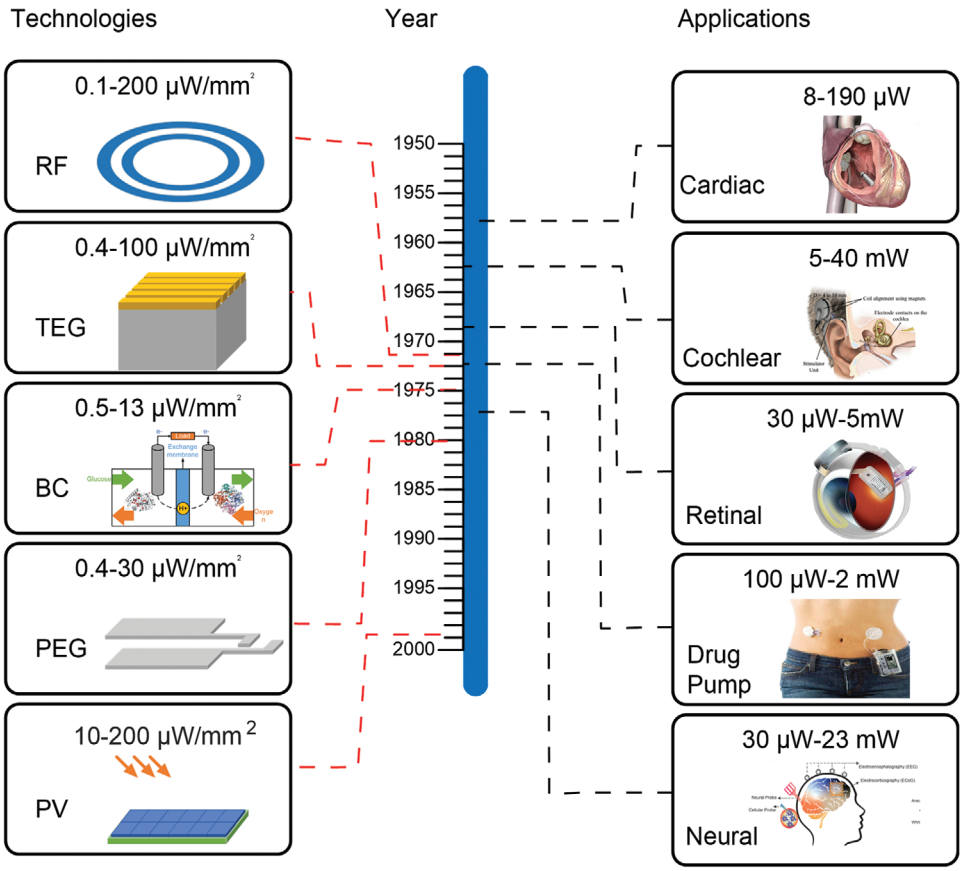

Figure 2. The time development of implantable power harvesters and implantable applications associated with their power range. The dates associating with dash line are the first appearance in the implantable applications, and the power range is based on the works, including power harvesters,[16,18,26,27,31–33,34] cardiac implant,[18,26,31,32] cochlear implant,[33] retinal implant,[16,31,34] drug pump,[31] and neural implant.[27,31] Reproduced with permission.[1,18] Copyright 2020, IEEE and Copyright Clearance Center.

these energy harvesters scavenge energy from the human body as well as the external environment, as shown in Figure 1a,[1] b,[11] c,[25] d[25,26] e,f.[27] Furthermore, we will discuss the latest developments in implantable PV cells and highlight the latest challenges in material synthesis, fabrication, encapsulation, and light penetration.

2. Overview

Figure 1g demonstrates the typical components of an implantable device. Variations in physical activity such as pressure and temperature can be detected via an implantable dedicated "sensing" block. The sensed signal can be processed by the signal processing block via an analog to digital converter. Next, the converted signal can be transmitted outside the human body via the "communications" block. All these mentioned blocks need to be supplied by power harvesting units that scavenge energy from the human body or from the ambient.[28] Moreover, all these blocks interface with biomedical sensors or actuators subcutaneously.[29] The data sensing and conversion blocks are able to detect the physiological data of the human body and transfer it into an electric signal.[30] These signals can be processed and stored as readable data by the signal processing module. Subsequently, all these data are transmitted and received through tissue using a signal communications block.

Our review will focus on the power harvesting technologies that can be used to sufficiently drive the electronic components in an implantable system. In this section, we will highlight the amount of power required by each implantable application, as well as the amount of power that can be scavenged using the different power harvesting techniques.

2.1. Implantable Applications

Figure 2 shows the power requirements of mature and emerging implantable systems, as well as the development of energy harvesters for implantable applications.[16,18,26,27,31–34] Generally, power requirements for implantable biomedical devices are in the microwatt to milliwatt range. Voltage requirements are in the range of 2–3V.[2] **Figure 3** shows the development of using PV cells for implantable applications.

In implantable device design, there are two approaches to optimizing power consumption and delivery. The first involves minimizing the power consumption in functional blocks, whereas the second involves increasing the power generation density. Several design techniques were investigated to improve the

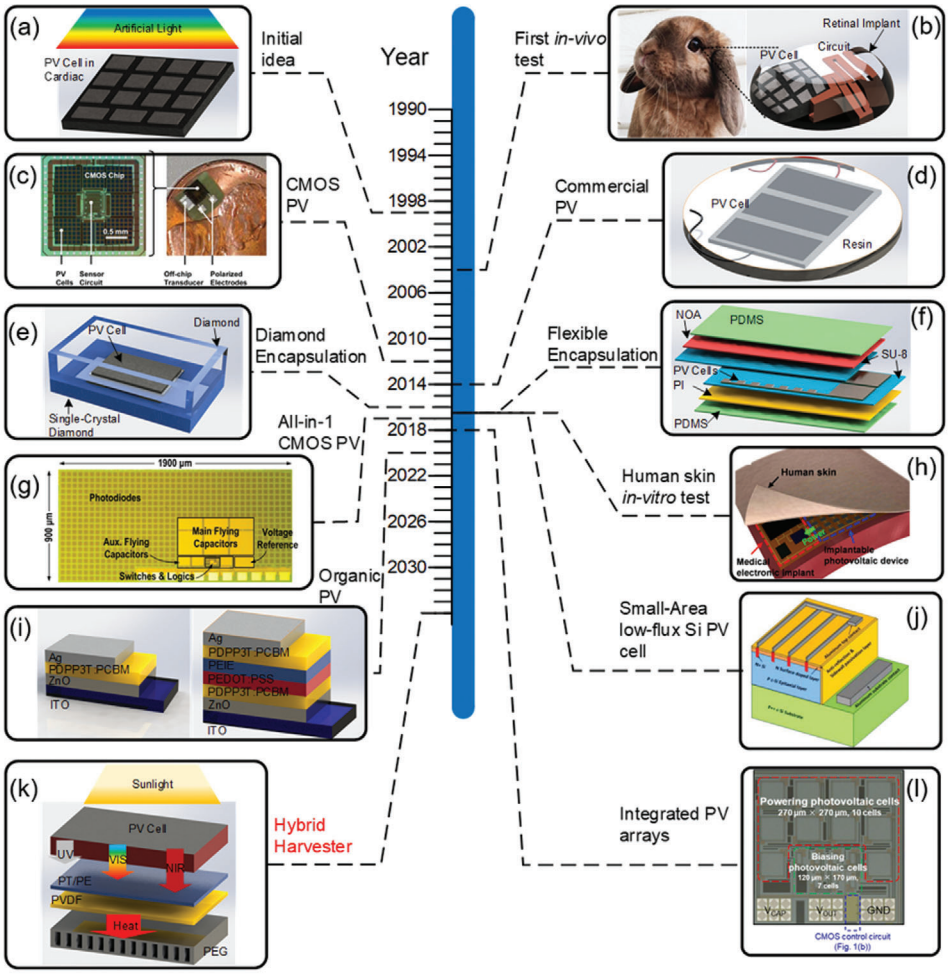

Figure 3. The development of the implantable PV cells from 1999 to 2030. With 20 years development, the implantable PV cells are developed from a proposed ideal to a mature technique with in vivo or in vitro test applied. 10 years development prospection (2020–2030) is also shown. a) The first proposed idea of the implantable PV cell.[85] b) The first in vivo test of the implantable PV cell in animal.[86] c) The first on-chip CMOS PV cells.[80] d) Using commercial PV cell to power a pacemaker.[87] I Diamond encapsulation of the implantable PV cell.[90] f) Flexible PV cell made by multilayer flexible encapsulations.[89] g) The stacked CMOS PV cells with power management circuit.[81] h) First in vitro test of implantable PV cell in human skins.[91] i) The first organic implantable PV cells (single-junction and tandem cells).[84] j) Small-area implantable PV cell in low-flux light condition.[103] k) Prediction of hybrid PV with the other harvesters to help merge the energy. l) Integrated silicon PV arrays bonding with CMOS circuit.[27] Reproduced with permission.[27,80,81,91,103] Copyright 2020, IEEE and Copyright Clearance Center.

performance of implantable devices, which include dynamic power-performance management and energy-efficient signaling.[28]

The dynamic power-performance management includes energy harvesting, energy storage, and voltage conversion. Energy harvesting and energy storage are used to extend the lifetime of the implantable device. The voltage conversion for an implantable device can optimize the voltage and current requirement of the loads.[28]

The energy-efficient signaling consists of low-power analog and digital signal processing. Low-power analog signal processing mainly reduces the power requirement of analog-to-digital conversion by adapting dynamic range and the inconsistency of the device. To mitigate the power loss from noise margin and distortion of the digital circuit, the low-power digital signal processing technique offers the reconfigurable and energy-efficient digital architectures. The techniques provide the possibility to increase the device lifespan and meanwhile decrease the power loss in the loading and signal processing.[28]

As mentioned above, minimizing the power consumption and losses can improve the lifespan of implantable biomedical devices. In one case study, it was shown that decreasing the power consumption of an implantable device from 10 mW to 8 µW increases the lifespan of the implantable medical device from 3 days to 10 years.[28,35] Low-power components enable greater device functionality, whereas increasing the number of functional blocks raises the power loads. In this case, the choice of power harvesting technology depends on the application. Therefore, before selecting a particular power harvester, it is necessary to investigate the specifications and power requirements of different implantable applications.

As mentioned above, cardiac pacemakers, cochlear hearing aids, drug pumps, retinal stimulators, and neural stimulators are mostly used in healthcare applications. The pacemaker was first

invented in 1958, and over 200 000 patients survive from cardiac dysrhythmias and heart failure using these devices.[9,10] The lifetime of pacemakers is normally 7–10 years, which requires years of operation on battery charging instead of surgical replacement (cost: $6000–$12 000).[2,9,28] The power consumption of the pacemaker is normally in the microwatts range, and the device requires minimal processing and low analogue-to-digital speed. For special requirements, some pacemakers require high-energy cardiac defibrillation, and the defibrillation has to be generated by using large and intensive electrical pulse.[9]

In 1961, House from Los Angeles first installed cochlear implants inside two patients with a hearing disorder. It was designed to support or restore functional hearing by involving electric stimulation. Compared to advanced implantable systems like the pacemaker (250 000 patients in USA[36]), over 200 000 people received implantable hearing aids.[37] In fact, the hearing aids market is largely attributed to the rapid development of power management technologies.[38] Power consumption is normally between 100 and 2000 µW. In comparison with the pacemaker and cochlear applications, the retinal and neural stimulators are emerging technologies. The power consumption of stimulators varies from the micro to the milliwatts- range according to the smart array configurations. The first neurological implant in mammals was created in 1976 by Stenevi.[39]

Similarly, retinal implants were designed to restore a rudimentary sense of vison for individuals with visual loss. They were first designed and implanted by Brindley and Lewin in 1968.[40] Similar to the neural stimulator, the power requirements of retinal stimulators were associated with the electrode array configuration. The drug pump system was designed in the 1960s and was developed to replace oral administration in specific therapies.[41] Compared to previous applications, the drug delivery system can be inserted into different body locations that include intraocular, intrauterine, and vaginal sites. The system must be surgically removed when the drug is exhausted which does not support applications as a long-term self-powered device.[14]

In the following sections, different energy harvesting methods that have been used for various implantable applications will be described. We discuss each technology's working principles, as well as its merits for meeting the power demands for implantable electronic devices.

2.2. Implantable Energy Harvesters

2.2.1. Kinetic Energy Harvesting

Piezoelectric energy harvesting involves converting mechanical energy to electrical energy. The direct piezoelectric effect is well-suited for power harvesting that will induce a piezoelectric potential attributing to the positive and negative charges of a polar surface if an external force is applied on the piezoelectric material.[2] The following coupled equation describes the piezoelectric effect:

$$S = SE \cdot T + dt \cdot E \tag{1}$$

$$D = d \cdot T + \varepsilon T \cdot E \tag{2}$$

where S is the strain tensor, T is the stress tensor, E is the electric field, D is the electric displacement, SE is the compliance under a zero or constant electric filed, ϵT is the dielectric permittivity under a zero or constant stress, and d and dt are the direct and reverse piezoelectric coefficients.[42]

The performance of piezoelectric systems is based on the characteristics of the piezoelectric material. The first implantable piezoelectric power system dates back to 1980.[43] To date, the most common types of piezoelectric material are zirconate titanate (PZT), zinc oxide (ZnO), and polyvinylidene fluoride (PVDF).[2] The first implantable PEG was fixed to a dog's ribs in 1984.[44] Spontaneous breathing lead to a PVDF cell producing 18 V and 17 uW of output peak voltage and power. PVDF material is advantageous since it is flexible and biodegradable, making it suitable for wearable and implantable applications.[45]

PVDF material has been widely used in implantable devices. In Yanhao's work, the PVDF piezoelectric generator was embedded with a polydimethylsiloxane package, and the whole package was implanted into rodent muscle. The stability of output was tested with an operating duration of 5 days. The average open circuit voltage (V_{oc}) and short circuit current (I_{oc}) were 3.8 V and 3.5 µA.[46]

In 2015, a novel flexible and implantable PVDF PEG with capacitor storage was proposed with a size of 56 mm × 25 mm × 200 µm. It was tested both in vitro and in vivo. For the in vitro case, The maximum power output (P_{max}), V_{oc}, and I_{sc} were 0.681 µW, 10.3 V, and 400 nA. As for the in vivo study, the maximum current and voltage were 1.5 V and 300 nA when the PEG was attached to the heart of a male domestic porcine. The output power became 30 nW after 700 ms duration with 70 bpm heart rate. This implantable PEG has shown the potential as power source for low-power implantable electronic devices in the future.[32]

Another PVDF piezoelectric study showed the in vitro and in vivo output power of 2.3 µW and 40 nW, respectively.[47] Other PEG materials are described in Khan et al. (2016)[45] and Shi et al. (2016).[48] Similarly, the output power for ZnO and PZT is in the nW and µW scale.[45,48] ZnO material was used for encapsulation with textiles to convert the wasted mechanical energy into electric energy. Due to its quartzite crystal structure, PEG in ZnO can work as a high-frequency resonator in microelectromechanical systems (MEMS) or nanoelectromechanical systems. The PZT is more commonly used compared with the other materials because of the lighter weight. Although PZT suffers from a toxic nature, it still validate in vitro and in vivo studies.[45]

A MEMS-based broadband piezoelectric ultrasonic energy harvester was previously developed to power implantable biomedical devices. The system was able to generate output power of 1.47 µW (with tissue) and 0.047 µW (without tissue), respectively.[48] Furthermore, this technique was FDA approved.[18] To avoid cytotoxicity of the constituent materials and immune response, PZT device could be encapsulated by bio-compatible materials. The power density of PZT mechanical energy harvester on the bovine heart in vitro demonstration could reach 1.2 µW cm^{-2} and output peak voltage is as large as 8.1 V.[49] Furthermore, piezoelectric sensors could harness environmental vibrations and convert them into electrical energy. For example, a 15 mm diameter PZT disc is involved to transfer ultrasonic transcutaneous energy and power the internal unit under a piece of pork muscle skin.[18,50] A power of 100 mW

with 39.1% efficiency is successfully transferred at 650 kHz and 5 mm distance. The PZT material was utilized because of high acoustic impedance. The acoustic matching layers were installed on the active surface of PZT material and the backside was left open to allow ultrasonic escape, which massively improves the coupling energy into tissue. A Gaussian excitation of transmitter approximation is applied to implement the ultrasonic to overcome the limitation of uniform excitation.[18,50]

Therefore, piezoelectric energy harvesters can be designed to be flexible and small to meet human body vibration requirements. However, PZT is still the most popular piezoelectric material in recent devices, which is brittle and toxic. Thus, more research is needed into advanced materials that are more flexible and lead-free. Another limitation of piezoelectric transducers is that they provide an AC voltage. Thus, an interface circuit is required to convert AC to DC electricity. This process increases system complexity and cost, and reduces the overall system efficiency.

2.2.2. Bio-Chemical Energy Harvesting

BCs use living organisms to generate electricity and were first demonstrated in implantable applications in 1974.[51] Biofuel cells use biocatalysts to produce power. These cells can convert bio-chemical energy to electricity via biochemical reactions. Living organisms in the human body have biofuels (e.g., glucose in blood) that are capable of generating power in microwatts range.[52] The biofuel is oxidized at the anode of the biofuel cells where the electrons are released, and the oxygen is reduced at the cathode. The catalyst in the biofuel cells can be an enzyme that can directly convert the carbohydrate chemical energy to electric energy.[52]

Mesoporous carbons are used for the anodic biocatalyst for glucose oxidation.[53] In 2009, Zhao et al. showed a comparison between the electrical performance of the biofuel cells based on the mesoporous carbons and carbon nanotubes.[53] The electric performance of mesoporous carbon-based structure was much more impressive than carbon nanotubes (CNTs) based structure, which are (V_{oc} = 0.82 V and P_{max} = 38.7 µW cm^{-2}) and (V_{oc} = 0.75 V and P_{max} = 2.1 µW cm^{-2}), respectively. Thus, it is a strong proof that mesoporous carbons will be the novel type of robust and advanced material for electrodes.[52,53] The biofuel cell is modified by DNA wrapped single-walled carbon nanotubes. It was found that the electric characteristics increased attributing to the immobilization of glucose oxidase and active site protection. Moreover, this novel structure will provide a tremendous power density of 730–760 µW cm^{-2} with a duration of a week and the stability of biofuel cells will be improved.[54] A dual power harvester combined with a TEG and biofuel cells was embedded with 0.18 µm complementary metal-oxide-semiconductor integrated circuit. Simultaneous maximum power extraction of two power generators is led to a control circuit to improve efficiency and diminish the switching loss. Both harvesters obtain remarkable electric power, which is 23 and 29 µW in TEG, respectively.[55] The biofuel cell was fabricated with Lac-GAfCs-MWCNTs/GC cathode and GOx-GAfCS-MWCNTs/GC anode, respectively, and the cell operates inside the membrane-separated acetate solution at pH 5. The output voltage, current density, and power density are 0.19 V, 114 µA cm^{-2} and 9.6 µW cm^{-2}, respectively.[56]

Among the issues with biochemical energy harvesting is the low power conversion efficiency, which means that a large area is required. This makes them infeasible for implantable power harvesting applications.

2.2.3. Thermal Energy Harvesting

Thermoelectric devices convert thermal energy into electricity via the Seebeck effect. The Seebeck effect is a thermoelectric phenomenon that involves converting a temperature difference into a voltage difference. This phenomenon mainly occurs in metals and semiconductors. Heating one end of a semiconductor causes a temperature difference, which enables carriers to diffuse from the hot to the cold ends of this semiconductor. Considering an n-type semiconductor as an example, due to the high concentration of electrons, the majority carriers will diffuse from the heated side to the cooler side in the semiconductor. The minority carriers (holes) will in turn move in the opposite direction. In open circuit conditions, negative charges at the hot end and positive charges at the cold end are formed at either side of the semiconductor, which results in an electric field to appear inside the semiconductor. When the semiconductor reaches a stable state, the electromotive force caused by this temperature difference appears at both ends of the semiconductor. Both p and n type semiconducting materials are required to cause current flow in a thermoelectric generator.

Thermal energy harvesting has been used in many sensing applications.[57] The thermoelectric effect can be described by the following equations:[26]

$$V_G = N \propto \Delta T \tag{3}$$

$$P_L = N^2 \alpha^2 \Delta T^2 \left(\frac{R_L}{R_L + R_{in}} \right) \tag{4}$$

where V_G is the output voltage, α is the Seebeck coefficient of thermal material, N is the number of the thermocouples, R_L is the loading resistance, R_{in} is the internal resistant of TEG and P_L is the output power. It is well known that the human body is an unlimited heat source, which leads to great potential in implantable energy harvesting.

The first implantable thermoelectric power harvester was demonstrated in 1970.[58] The most common semiconductor material for thermoelectric power harvesting is polycrystalline silicon germanium (poly-SiGe) and bismuth telluride (Bi-Te). However, due to its high ZT properties and room temperature fabrication capabilities, Bi-Te is mainly used for commercial applications.[59] In comparison to poly-SiGe, Bi-Te can generate between 19 and 30 µW mm^{-2} with 27–70 K temperature difference.[60]

Thus, thermoelectric generators have many advantages that include its lightweight and flexibility. However, these energy harvesters are not ideal in environments that have a similar temperature to the human body.[61]

2.2.4. Radio Frequency Energy Harvesting

Radio Frequency energy harvesting involves scavenging power from electromagnetic radiation. The first RF energy harvesters were demonstrated in pacemakers back in 1969.[62] RF waves can be classified as near-field or far-field, depending on the electromagnetic waves in the different distance (specified by Fraunhofer distance).[63]

Near-field RF power harvesting can be described using the following equations:[64]

$$P_{\text{in}} = \frac{M}{L_{f1}R_2}\left(\frac{M}{L_f}V_1 - V_2\right)V_1 \tag{5}$$

$$P_{\text{out}} = \frac{1}{R_2}\left(\frac{M}{L_f}V_1 - V_2\right)V_2 \tag{6}$$

where M is the mutual inductance between the transmitting and receiving coils, L_f is the inductance of transmitting coil at frequency f, V_1 is the supply voltage at transmitting end, V_2 is the charging voltage at the receiving end, R_2 is the resistance at the receiving end. The far-field RF power harvesting can be described as following equation:[63]

$$P_{\text{out}} = \frac{P_{\text{T}}G_{\text{T}}G_{\text{R}}\lambda^2}{(4\pi R)^2} \tag{7}$$

where P_{T} is the power in transmitting antenna, G_{T} and G_{R} are the transmitter and receiver antenna gain, respectively. λ is the wavelength of the electromagnetic wave.

A neural interface microsystem was powered by an inductive link at 2 MHz which was supplied by a Li-ion battery.[18,65] The power link consisted of a 210-pF ceramic capacitor and a 27-turn 27 mm AWG 40 strand Litz wire with the inductance of 2 μH. Such coil was advantageous of a high-quality factor (Q) of 75.4 with 2 MHz.[18] A Copper based on the ceramic coil was embedded in a 9 mm^2 chip which is implanted in human retinal to produce artificial vision. Five subjects such as light perception, localization and motion detection were tested by patients. The copper in the polyimide coil was applied at the far-field frequency of 910 MHz was operated. In this case, the possibility of RF energy harvesting inside moving small animals was approved and the completely wireless behavior can be controlled.[18,66] Energy was coupled from a copper power link in Ferro solution to resonant energy into a head borne device a maximum magnetic field of 300 A m^{-1}. These in vivo experimental results were tested in a rat inside a cage-like power transducer at a resonant frequency of 120 kHz. The device was orthogonal to the cage to optimize the magnetic coupling.[18,67] In 2010, two on-chip antennas were embedded with circuit by using 0.18 µm technology. A remarkable power scavenging distance of 7.5 cm was achieved, and meanwhile 13.2 µW cm^{-2} power was harvested by the downlink. There was no-off chip components used in this research.[68] In 2011, a loop antenna was applied in an intraocular monitor, and the biocompatible methacrylate plastic and small size make it as a good candidate in retinal application. The power density of 28.33 µW cm^{-2} was achieved in 1.5 cm at −10.5 dBm RF sensitivity.[69] In 2018, the circular polarization was considered in antenna design, and the antenna had a relatively smaller size and can obtain a better electromagnetic radiation. After tested under a 4 mm skin, 9.65 µW cm^{-2} power density was obtained in a distance of 40 cm at 915 MHz.[70]

It must be emphasized that the power density of near-field RF is unpredictable compared with far-field RF, which is normally considered as uniform.[63] The different magnetic flux density in near-field and far-field range make the RF harvester facing different challenges associated with these ranges. The near-field RF requires perfect impedance matching and antenna alignment, which is still a challenge for designers. According to the low far-field magnetic flux density, it is difficult to harvest sufficient energy to start up the circuit by using far-field RF harvester, where the start-up thresholds are different in different CMOS technologies.[71] In addition, the frequency of far-field RF harvester is limited up to GHz range as a result of tissue loss.[71]

2.2.5. Photovoltaic Energy Harvesting

Harvesting energy from light has been used for powering portable consumer products. Here, PV cells are used to convert light or the sun's energy into useful electricity. Ultimately, semiconductor materials are commonly used for the purpose of producing currents and voltages as a result of the absorption of light, which is a phenomenon known as the photovoltaic effect. Most PV cells are fabricated from either monocrystalline or polycrystalline silicon (Si) materials. In its most basic form, a PV cell consists of a pn-junction diode. Typical PV cell efficiencies range from 18% for polycrystalline to 24% from highly efficient monocrystalline technologies.[72] These high-end PV devices typically include special light trapping structures that absorb as many of the incident photons as possible.[20]

The I–V characteristics and the output power of a typical PV cell can be described by:[73]

$$I(V) = I_{\text{sc}} - I_{\text{d}} - \frac{V + I(V)\,R_{\text{s}}}{R_{\text{sh}}} \tag{8}$$

$$P_{\text{out}} = I_{\text{sc}} \cdot V_{\text{oc}} \cdot \text{FF} \tag{9}$$

Where I_{sc} is the short-circuit current, I_{d} is the dark current, R_{s} is the series resistance of PV cell, R_{sh} is the shunt resistance of PV cell, V_{oc} is the open-circuit voltage and FF is the fill factor.

For implantable power harvesting applications, PV cells cannot harvest in vivo bioenergy directly, but it can harvest energy from an ambient light source (natural light or artificial light).[74]

In this section, we will initially demonstrate the development of implantable PV cells. We will also compare PV cell performance using different materials and technologies. Next, the fabrication process of PV cells and the encapsulation techniques will be discussed. Here, it is important to emphasize that encapsulation involves protecting the PV cells as well as reducing the adverse side effects to humans. We will mainly discuss the transmissivity, flexibility and biocompatibility of the encapsulation material. Optical losses due to tissue scattering effects will be analyzed and the optical properties of different skins will also be summarized.

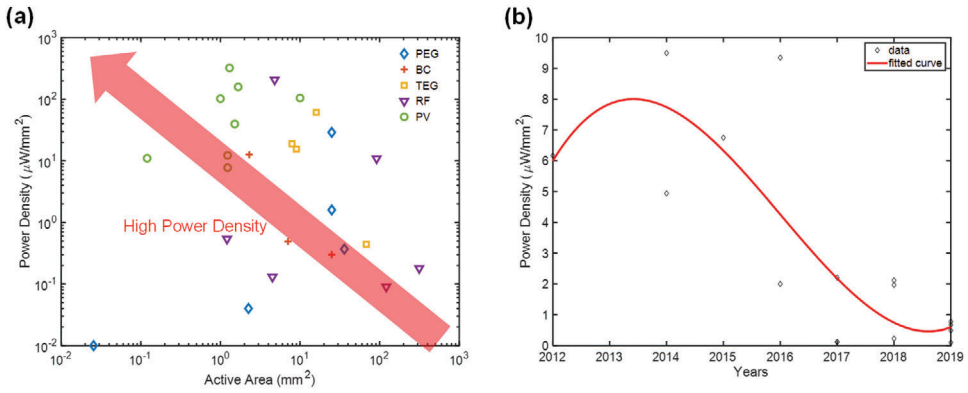

Figure 4. a) The normalized power from the different implantable power harvesters according to the active area of the devices, where the piezoelectric generator (PEG), biofuel cell (BC), thermoelectric generator (TEG), radio frequency harvester (RF) and photovoltaic (PV) cell are included. All the harvesters were tested in in vivo and in vitro, and the PV cells were under in vivo and in vitro testing under different light density. b) The harvested power changes of the implantable PV cells from 2012 to now.

2.3. Comparison between Implantable Power Harvesters

Figure 2a–j demonstrates the power consumption of various implantable devices and the harvestable amount of power by different technologies. The voltage requirements for a commercial implantable device is 2–3 V.[2] Batteries can satisfy the power and voltage requirements for implantable devices. However, their large size and weight restrict their use. In addition, there are chemical leakage risks that can cause damage to the body.[75] Thus, for an implantable power harvester to be effective, it must have a smaller size, better lifetime and provide sustainable power.

Figure 4a shows a comparison between the power density that can be generated from different power harvesting approaches. Clearly, implantable PV cells can harvest the highest power density. RF energy harvesters can generate high power in the near-field, but careful alignment is necessary. Far-field RF harvesters are inefficient when the frequency is increased to tens of GHz. The start functioning and magnetic field mismatch are the main constraints.[63,71,76] To be specific, the RF system requires power to wake up the system because the CMOS components always have a threshold, but far-field RF harvesters are inefficient. A perfect match between transmitting and receiving coils can increase the magnetic flux density, hence improve the power output. Large coil size, short power range and tissue losses are lingering challenges.[18,77]

As discussed before, PEG can harvest kinetic energy from human motion.[45] As can be seen from Figure 4a, the size of PEGs is larger than PV cells, BCs, and TEGs. Some PEGs have a small size, but the harvested amount of power is low. Another problem of PEGs and triboelectric nano generators (TENGs) is the unstable and low output voltage. Both these technologies need to be implanted into moving organs such as the heart, lungs, or in the pericardial region. However, the size, rate and external force of the organ affects the output voltage of the PEGs.[2] Notice that similar to PEG, TENG is a new type of kinetic energy harvester based on the conjunction of triboelectrification and electrostatic induction.[6] Such an energy harvester can be driven via rat breathing, thus enabling in vivo power delivery to the pacemaker.[6] Besides, the TENG has also been used to scavenge energy from the heartbeats of a porcine and was able to supply power to a real-time cardiac monitoring system.[78] Yet, both refs. [6] and [78] only provide limited data and cannot be directly compared using Figure 4a.

BCs are highly biocompatible with living organs, since they are often tested with plants, insects, and even mammals.[55,79] According to Figure 4a, the amount of harvestable power from BCs is similar to PEGs, but their size is relatively small. Although BCs are advantageous due to cheap fabrication costs and high biocompatibility, the degradation of the enzyme is still a challenge. Compared with other power techniques, TEGs highly depend on the temperature changes, but the maximum temperature difference in human body is less than 6 °C.[26]

Implantable PV cells have commonly been used as small-scale harvesters and have been demonstrated to generate power from ambient light. In addition, the introduction of light management techniques, power management circuits, MPPT control logic and start-up circuits will tremendously improve the performance of implantable solar cells.[24,80,81] Most importantly, new developments in solar cell technologies have enabled multicrystalline PV cells to achieve an efficiency improvement from 21.9% to 22.3% within one year (2017–2018). Furthermore, new and emerging materials such as perovskite have enabled a 1.2% increase in solar cell efficiency.[82]

3. Implantable Photovoltaic Cell

3.1. Development of Implantable PV Cells

Concerning the development of implantable PV cells, several improvements have been made with respect to materials, device configuration, encapsulation and stability. The major milestones of these developments are shown in Figure 3. The development in power density of implantable PV cells in terms of harvestable power changes since 2012 is depicted in Figure 4b. Before 2012, implantable PV cells occupied a larger area due to the CMOS technology available at the time. Between 2010 and 2014, implantable PV cell technology developed according to advancements in CMOS technology.[80] The on-chip PV cell was invented during this period.[80,83] Between 2014 and 2018, the literature

Table 1. A comparison of different types of Implantable PV cells.

Types	Material	Source	Light density [W m^{-2}]	Power density [mW cm^{-2}]	Package	Flexibility	Biocompatible	Application	Reference
Crystal	Mono-Si	Outdoors	1000	4.94[b)]	Silicone	No	Yes	Cardiac	[87]
	Mono-Si	NIR	2000	2.21[b)]	PLGA	Yes	Yes	LED	[104]
	Mono-Si	NIR	1000	2.13[a)]	–	No	No	Temp.	[100]
	Mono-Si	simulator	1360	6.17[a)]	–	No	No	Sensor	[80]
	Mono-Si	Halogen	12.2	18.87[b)]	–	No	No	–	[81]
	Mono-Si	NIR	7000	9.35[b)]	Diamond	No	Yes	Cochlear	[90]
	GaInP/GaAs	AM1.5G simulator	1000	8.46[b)]	PDMS	Yes	Yes	Cardiac	[89]
	GaAs	NIR	1500	44.12[b)]	Silicone/resin	Yes	Yes	Retinal	[86]
	GaAs	μ-ILED	430	42.29[b)]	–	No	No	Neural	[102]
Non-crystal	a-Si	Halogen	100	0.95[b)]	Silicone	No	Yes	Cardiac	[85]
	a-Si	Outdoors	1000	0.06[b)]	Silicone	Yes	No	Temp.	[105]
	Organic	NIR	1000	3.84[b)]	–	Yes	Yes	Retinal	[84]

[a)] On-chip PV cells; [b)] Off-chip PV cells.

showed a shift toward lower power density PV cells. Perhaps this could be attributed to an increased commitment toward better biocompatibility and encapsulation issues. After 2018, emerging technologies such as organic PV cells were demonstrated in implantable applications[84] without encapsulation.

Among the first researchers to propose the use of PV cells for implantable applications was Dan Tchin-iou in 1999.[85] A source providing light in the visible range was used to power a commercial solar cell with an integrated battery pack. This system was used to power an artificial heart. However, this research lacked analysis of tissue loss and under-skin device validation (in vitro or in vivo). In addition, the light source was confined to wavelengths in the visible range and did not consider light in the red and infrared ranges.

The first in vivo testing of an implantable PV cell was achieved by Thomas Laube in 2004.[86] A near infrared (NIR) light source was used and PV arrays were encapsulated with a resin. The PV cells were embedded in an intraocular microsystem, and the whole chip was implanted into a rabbit. The system was tested in vivo for 7 months, which is the longest testing duration for any implantable device to date. In addition, full information about the surgical procedure and recovery treatment were provided.

Between 2004 and 2012 there were no published articles in the area of implantable PV cells. During this period, implantable PV cells were discarded energy harvesters due to their size and due to the risk of infection from the connecting wires. However, thanks to advancements in integrated CMOS technology, there has been a renewed interest in using PV cells in 2012. In fact, Sahar Ayazian proposed a self-powered and fully integrated system, which embedded power-harvesting PV cells and sensor arrays in a 2.5 mm × 2.5 mm CMOS chip. They demonstrated successful power harvesting in the microwatt range for a device that was implanted 3 mm below chicken skin. They tested the feasibility of using a CMOS PN junction as a potential PV power harvester.[80]

Furthermore, Haeberlin et al. successfully demonstrated a PV driven pacemaker using thin film silicon materials ,[87] which was tested in vivo tested for 40 days in 2015.[88] The power density of their device was 0.95 mW cm^{-2}, as shown in **Table 1**. To scavenge more power, expensive semiconductor materials such as GaAs and GaInP, are needed.[89] The power density of GaInP/GaAs was 8.46 mW cm^{-2} under AM1.5G condition.[89] The GaAs PV cell achieved higher power density of 44 mW cm^{-2} by using NIR light source.[86] However, a better encapsulation would be required due to the toxicity of these materials. For example, Ahnood et al. demonstrated a diamond capsule for implantable PV cells, which was used both as a package and an optical window due to its high mechanical robustness, biocompatibility, and wide transmission spectrum.[90]

Considering the comfortability of the patient, flexible PV cells are used in the Implantable system by Song et al. in 2016. The PV cell was encapsulated with polymethyl siloxane (PDMS). The device can successfully supply a commercial pacemaker in a rat with the power of 8 mW cm^{-2}. To test the biocompatibility of the device, the amount of Arsenic was measured by using a mass spectrometer, and the 0.02 μg leakage by using emerging PDMS is lower than the daily intake from air breath (0.6 μg) and water (20 μg) by a person.[89] As the power output of the PV cell highly depends on the feature of covered skins, it is necessary to test the performance of the cells under human skins even if there are a lot of studies showing the viability in the animals. In this case, the performance of the PV cell under fresh and fixed human skins were measured in different location in 2017. The results (2.34 mW cm^{-2} under inner arm, 2.21 mW cm^{-2} under hand dorsum, 0.96 mW cm^{-2} under forehead) shows that the device under inner arm can provide most power output within same incident optical power.[91]

Organic PV (OPV) cells were also used for retinal applications due to their sensitivity to NIR light.[84] The authors demonstrated both single-junction and tandem OPV cells based on a bulky heterojunction. They investigated the voltage and storage charging time of the stimulating electrode in a saltine solution via electrical pulses. Since the V_{oc} of tandem PV cells (1.31 V) was higher than that of single-junction PV cells (0.67 V), the tandem PV cell was able to provide a full charge per pulse stimulation window in NIR light conditions. In addition, the efficiency of the tandem PV cell was higher (5.6% in comparison to 5.3% in the single junction).

For safety concerns, the light intensity in retinal applications was limited from 150 to 600 mW cm^{-2}. In this scenario, the tandem OPV with an active area from 2500 to 6250 μm^2 and electrode diameter of 35 µm can efficiently tune the charge per pulse, while the electrode of single-junction OPV was 60 µm, which limits the implantable resolution.

In summary, commercial PV cells were tested in vivo and used for implantable applications between 2000–2010. In effort to reduce the size of these cells (and increase the power density), CMOS technology was used after 2010 for fabricating both the on-chip PV cells and the power management circuitry. In the period between 2014 and 2017, researchers began using implantable PV cells to power real devices such as pacemakers. Moreover, encapsulation materials were used to protect device and ensure it is biocompatible. During this period, in vivo testing in animals and in vitro testing in human skin types were undertaken. Since 2018, emerging PV technologies such as organic PV cells were used in implantable applications.

3.2. Material and Technologies

Implantable PV cells harness light in the NIR range more effectively due to scattering losses from tissue.[75] However, there are issues with heating as a result of NIR light, which might cause discomfort to the wearer.

PV cells can be divided into two broad categories: crystalline and non-crystalline materials. Crystalline solar cells are typically more efficient, more expensive and less flexible than non-crystalline materials.[92] In 2015, around 93% of all PV cells were made from crystalline silicon materials, with 24% of this share from monocrystalline Silicon and 69% from multicrystalline Silicon.[93] Today, almost 89% of solar cells are fabricated from crystalline silicon, 10% from amorphous silicon and 0.5% of Cadmium telluride, dieseline, copper indium and gallium arsenide.[94] Table 1 compares the output power density, flexibility, biocompatibility between the different material or technologies.

Due to their mature technology, Si, GaAs, and GaInP are typically used in implantable applications.[81,89,95] Compared with silicon, gallium is a soft metallic material that is often combined with a compound such as As, N and P. Such materials are often called III-V compound semiconductors.[96] Gallium arsenide (GaAs) is particularly suited for NIR light absorption due its higher bandgap and lower reverse saturation current. Consequently, these materials normally have a better EQE in the NIR region, while amorphous silicon (a-Si) is better suited to visible light.[97] Moreover, due to the issues with heating, GaAs is less sensitive to heating (0.14 to 0.15 Ohm resistance variation based on the temperature coefficient from 0 to 50 °C[98]) and has a higher breakdown voltage. For instance, the breakdown voltages of GaP and GaAs at 10^{15} cm^{-3} doping gradient are approximately 800 and 300 V in comparison to 200 V for Si.[99] However, the toxicity and higher cost are the main limitations.

Apart from wafer-based PV cells, biodegradation of thin-film silicon PV cells have been investigated in different conditions.[97] In comparison to the cutting and sawing process of wafer-based cells, the fabrication of the thin-film cell needs microelectronics processing techniques.[97] The most common materials used for thin-film PV cells are a-Si, microcrystalline silicon (μc-Si), and mono crystalline silicon (c-Si). During the fabrication process, c-Si thin film cells are formed using the transfer printing process, while a-Si and polysilicon thin films are formed using the chemical vapor deposition (CVD) process. In contrast, OPV cells are advantageous due to their high flexibility, low cost and ease of fabrication.[92] They can be a good candidate for implantable applications if the energy conversion efficiency can be improved, and the stability of the cell can be prolonged.

Currently, there are two types of PV cell architectures that are used in implantable applications: CMOS[27,75,80,81,86,89,91,95,100–104] and commercial PV cells.[85,87,90,105] Table 1 compares the output power density, flexibility, biocompatibility between the different materials and technologies. On chip PV cells are fabricated using standard CMOS technology, which applies the diode formed by N+ region, P+ region, N well, p well, deep N well and p substrate. **Figure 5**a,b demonstrates a PV cell design with circuitry based on CMOS technology.[106] One P+/N-well PV cell and one N+/P-sub PV cell were used as the PMOS source and NMOS source. Each PV cell was able to supply 0.3–0.4 V and different configurations of PV cells can provide different voltage output.[81,106]

During the fabrication process, the CMOS circuit is often shaded by a metal layer to avoid leakage of photo-generated current in the circuit. In fact, the on-chip PV cell occupies a smaller area than an off-chip cell, since all the components are integrated into a single block. However, the efficiency of on-chip PV cells is typically lower (<20%) and the negative voltage formed by reversed junctions and the P substrate connected to ground makes it difficult to make different PV cell configuration.[81]

Figure 5b shows a PV cell fabricated in the laboratory instead of using CMOS technology.[89] Compared with the conventional use of monocrystalline silicon and the limited stacking topologies of CMOS technology, off-chip PV cells can be based on a variety of materials (inorganic and organic) and stacking topologies. For instance, heterojunction PV cells were previously fabricated using GaInP/GaAs materials in a 2 x 7 array to drive a load.[89]

CMOS technology can also be used to fabricate off-chip PV cells by thinning the p-type substrate to 60 µm[75] and back illuminating the cell. In that case, instead of grounding the substrate, it is left floating. Furthermore, it would not be possible to integrate this off-chip PV cell with other power management circuitry due to this to floating substrate. Figure 5c,d shows two types of off-chip (back-illuminated) PV cells[75] with an improved efficiency of 18.3%.[75]

3.3. Encapsulation

Encapsulation is necessary to prevent the electronic circuitry from corrosion. Conventional encapsulation is based on ceramics, glass and metals, such as the Titanium and ceramic packaging. In the pacemaker and other similarly packaged implants, most of the titanium shell is exposed to body fluids. This is acceptable if all exposed metal surfaces (including tracks) are at the same potential. Such implants sometimes use metal in glass feedthrough, although this is becoming common.[94]

Metals, glass and ceramics are highly biocompatible materials. They are stiff and have a low permeability to water vapor.[107] Although these conventional materials are advantageous in harsh

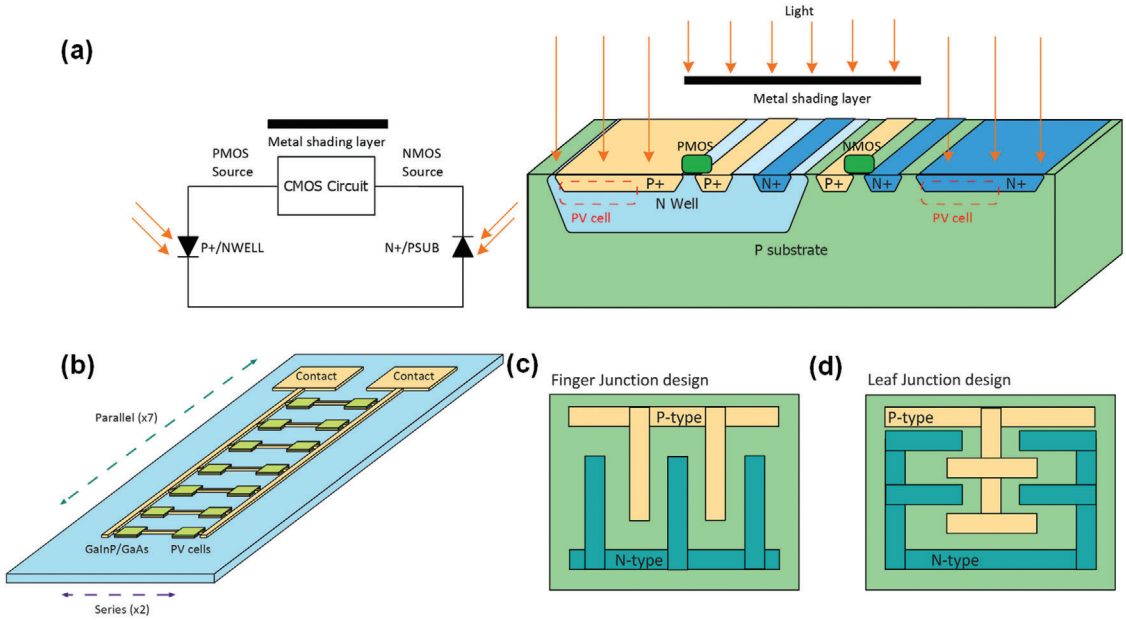

Figure 5. The structure of the implantable PV cells: a) the equivalent circuit and cross-section of the integrated PV cells with circuitry fabricated by CMOS technology,[106] and b) a home-made PV cells 2 × 7 arrays in GaInP/GaAs according to the work implemented.[89] c,d) The unit cell layout views of the finger type and leaf type junction designs: Finger-type junction design in CMOS on-chip PV cell (c) and Leaf-type junction design in CMOS on-chip PV cell (d).[75]

physical environments, they are not compatible with the CMOS fabrication process.[107,108] Consequently, novel encapsulation materials have been investigated such as SiO_2, SiC, Al_2O_3, diamond, as well as organic silicone polymers, polyimide, PDMS, liquid crystals and SU-8.[108] The parameters of these emerging materials are shown in **Figure 6**a–d.

There are two types of implantable encapsulation methods: 1) encapsulation for a conformal layer, 2) encapsulation for an impermeable envelope. As shown in **Figure 7**a,b, the encapsulation and packaging techniques are predominantly composed of Hermetic packages and polymer encapsulation. The polymer encapsulation is one of the highly reliable techniques to protect the electronic components from the subcutaneous environment, which is shown in Figure 7b.

Soft encapsulation typically provides greater comfort to patients.[109] Silicone rubber is attractive in this encapsulation technique because it can greatly prevent the ambient fluid from shorting conductors and long-duration corrosion damage from water vapor.[109] However, the cleanliness and absence of voids are still challenging to obstruct the performance the implantable electronics. To avoid these problems, the adhesive connection between the layers in the encapsulation must maintain strong for the whole required lifetime of the implantable device. If the adhesive layer is not strong enough, the pressure caused by ionic liquid outside will damage the adhesive bond and drive the water vapor into the voids in the encapsulation, which causes the increase of humidity inside of the encapsulation. Besides, the polymer encapsulation is tremendously reliable when the large-size discrete components in simple circuitry are applied.[109] Nowadays, the integrated circuit (IC) is routinely applied as a part of an implant. It is quite necessary to investigate the ability of polymer encapsulation alone to protect the bare IC chips, otherwise, this technology will only be adaptable for the short-term and medium-term implantable applications.[109] The Hermetic package is based on a solid water-impermeable shell and hermetically sealed, which is shown in Figure 7b. The hermetic package can protect the electronics from the ambient fluids and maintain the humidity at a low level. However, it requires the material to be impermeable to vapor.

When considering the encapsulation of photovoltaic-driven implantable devices, there are three factors which can significantly influence the selection of novel materials: optical properties, biocompatibility, flexibility and lifetime. Figure 6a–d shows the variation in the physical properties of the encapsulation materials. Figure 6a shows the variation in the refractive index of the encapsulation materials as a function of wavelength for the following materials: Crystalline alumina (α-Al_2O_3),[110] thin-film alumina,[110] hafnium oxide (HfO_2),[111] fused silicon dioxide (fused SiO_2),[112] crystalline SiO_2,[113] thin-film SiO_2 ,[114] diamond,[115] polyimide,[116] parylene,[117] silicone (PDMS),[110] liquid crystal polymer (LCP).[118] Similarly, Figure 6b shows the variation in the extinction coefficient as a function of wavelength for the same range of materials. It is noteworthy to mention that the refractive index of these materials is close to 1.5 in the visible and NIR region, which is very close to the refractive index of human skin.[119] In addition, the extinction coefficient of the materials is close to 0 in the visible and NIR range, meaning that the absorption of the light is small and achieving high optical transmittance.

In Figure 6c, the lifetime and mean time to failure (MTTF) of the encapsulation materials are shown for the following materials: Al_2O_3,[108,120] HfO_2,[108,121] SiO_2,[108,122] polyimide,[108,123] parylene,[108,124] silicone,[108,125] and LCP.[108,124] The MTTF of these materials is obtained by placing them in a specific

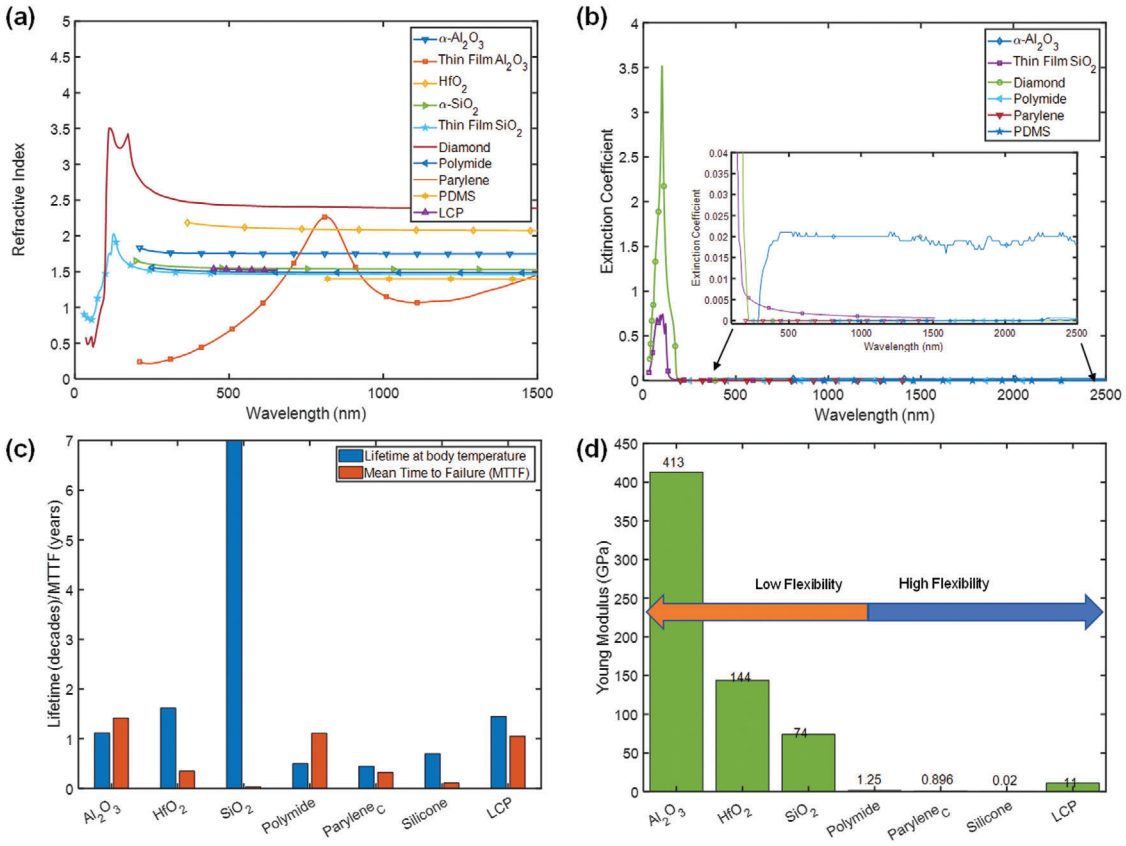

Figure 6. Variation in the encapsulation material properties: a) refractive index as a function of wavelength, b) extinction coefficient as a function of wavelength, c) lifetime in body temperature and mean time to failure, as well as d) Young's modulus.

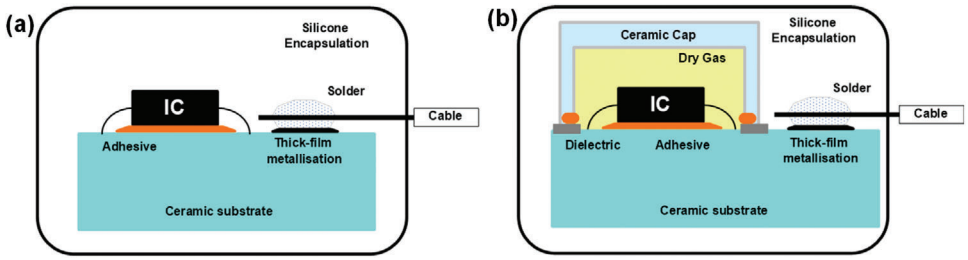

Figure 7. Two types of implantable encapsulation or packaging: a) polymer encapsulation, which is applied in the implantable devices, and b) the hermetic package which is applied in the implantable devices.

temperature, and the long-term reliability is validated by placing the samples in a saline solution in accelerated aging experiments. The lifespan of these materials in the human body can be obtained from the MTTF values (reaction rate in saline solution) and other properties of the materials. It is clear that inorganic materials such as Al_2O_3, HfO_2 and SiO_2 have longer lifetimes than organic materials, since they are more sensitive to sterilization than their inorganic counterparts.[108]

The flexible encapsulation of the chip can massively increase in fracture strength of up to 190% and curvature of bending 85%.[126] To understand the flexibility of the encapsulation, it is significant to examine their mechanical properties. Figure 6d shows the variation in the Young's Modulus for different materials. Generally, a high Young's modulus means the material is difficult to bend and has poor flexibility according to same geometry.[126] The geometry also influences the flexibility. For example, a ultra-thin chip with thickness <20 µm have been investigated to obtain a compact high-performance flexible electronics.[126] **Table 2** shows the fabrication processing and physical properties of the encapsulation materials.[108] The physical properties such as thermal expansion coefficient, resistivity and moisture absorption are factors that affect the biocompatibility of the encapsulation. We will discuss the different types of encapsulants in the following paragraphs.

For example, alumina (Al_2O_3) is considered as a good encapsulation material with high biocompatibility, and it typically works

Table 2. A comparison of different types of encapsulation material.

Material	Technologies	Thickness [μm]	Thermal expansion coefficient	Moisture absorption [%]	Flexibility	Failure criteria [nA]	Resistivity [Ω m]
Al_2O_3	ALD+CVD	6.052	4×10^4 °C^{-1}	4.75 at 30 °C	No	1	–
HfO_2	ALD	0.1	–	–	No	1	–
SiO_2	Thermal	0.1–1	4.5×10^4 °C^{-1}	6.04 at 30 °C	No	–	–
Diamond	CVD	300	–	–	No	–	–
Polyimide	Spin coating	10	40 ppm °C^{-1}	3	Yes	1000	10^{16}
Parylene C	CVD	6–40	35 ppm °C^{-1}	–	Yes	1	8.8×10^{16}
Silicone	CVD	40	340 ppm °C^{-1}	–	Yes	–	2.9×10^{16}
PDMS	Spin coating	150	–	–	Yes	–	–

as the feedthrough with a titanium package.[108] It provides a good moisture barrier and demonstrates high RF transparency. Alumina offers conformal coverage over a surface and provides pinhole-free films.[108] However, this material requires a labor-intensive process for assembly and has similar miniaturization issues with metals and glass.[108] Moreover, Alumina exhibits an extinction coefficient of null at 635 nm and a refractive index of 1.77 at 635 nm.[127] Moreover, the inorganic encapsulation process is based on CVD. For instance, the Al_2O_3 is normally deposited by ALD and CVD, SiO^2 combines Thermal bonding and CVD. However, the organic encapsulation formation including polyimide, silicone, PDMS, LCP is normally achieved by using spin coating, thermal bonding.[108] Despite the Parylene C, it normally applies CVD for complex surface topography with crevices and sharp edges.[108]

Other materials include HfO_2, which is often applied as the conformal coating over nanoscale devices using the atomic layer deposition (ALD) technique. It has great thermal, mechanical, and chemical stability.[108,128] It also exhibits a null extinction coefficient from 300 to 10 000 nm with a refractive index of 2 (5000 nm)–2.18 (365 nm).[127] Recently, HfO_2 was involved in hermetic packaging to be the extra moisture barrier between the organic layers or working as a multi-stack in the encapsulation layer.[129]

Silica (SiO_2) is typically applied in laser welding and anodic bonding. However, minimization is an issue for this encapsulation material.[108] Deposition of the SiO_2 layer uses the same CVD and ALD techniques as PV cells.[122] The refractive index of silica is 1.52–1.65 (198–2000 nm) and the absorption coefficient is 2.63. In that case, the transmittance is 99% for a 1 μm thick material and drops to 77% when the thickness is increased to 1mm.[130]

Diamond is an emerging biomedical encapsulation material due to its mechanical stiffness, wear and chemical resistance.[108,131] The encapsulation process requires high temperature and pressure. Its optical properties makes them ideal for implantable PV cells.[90] Ahnood et al. demonstrated CVD grown diamond plates to form the substrate. The optically transparent single crystal diamond was applied as the optical window layer of the encapsulation. The electrode interconnection to the PV cell was installed in the window top layer.[90]

Moreover, Polyimide has a thermal expansion coefficient of 40 and has 2–3% vapor absorption. Polyimide is normally applied in neural implants.[108] The polyimide can be compatible with the majority of MEMs processes (photosensitive polyimide in photolithography and polyamide adhesion in bonding). Parylene is advantageous in a thin conformal layer, it is flexible, inert and has excellent optical transparency (the refractive index and extinction coefficient are shown in Figure 6a,b). Until now, polymer encapsulation was mostly used for implantable PV cells due to its flexibility. The materials of these encapsulations are silicone, PDMS, PLGA and the other polymers. For example, GaInP/GaAs PV cells were capsulated with multilayers of biocompatible and transparent polymers, including 2 μm of SU-8 and 100–200 μm of PDMS.[89] The simple and flexible structure of these polymers make them mechanically compatible with human tissue, and the adhesive layer can prolong the lifetime of the package.[89]

Silicone is commonly used as a encapsulant for optical devices such as LEDs, photodetectors and PV cells due to its transparency and wide refractive index range (1.38–1.58).[132] Moreover, silicone meets the typical requirements of the healthcare and electronics industries due to its low dielectric constant (2.68 at 100k Hz), high thermal conductivity (0.4–1.34) and low resistivity (2.9×10^{14} Ω m).[132] For encapsulation purposes, silicone rubber provides good protection in the comfort layer, and it can be integrated with a ceramic material to develop an impermeable envelope. The advantages of silicone are as follows: 1) The outer layer is biocompatible, and the sharp layer is covered to protect the host body. 2) Corrosion of the exposed metal electrode is prevented from corrosion. 3) Silicone insulates the feedthroughs that carry the signal in and out of the sealed enclosure. In addition, Silicone can be applied as the sealant of frame and junction box for PV cells.

3.4. Skin Properties and Losses

Skin aims to protect the internal organs from light. Consequently, harvesting energy from ambient light using implanted PV cells becomes a challenge. Thus, light will be attenuated due to tissue losses. Furthermore, different skin types will attenuate light differently.[133] In this section, the properties of different skin types will be explained, and the influence this has on the performance of implantable PV cells will be demonstrated.

Skin is a complicated medium, and its optical parameters dynamically vary with temperature, hydration and radiation. Furthermore, light propagation through skin depends on absorption, scattering, transmission and reflection between tissue boundaries. These boundaries are the interfaces between two media

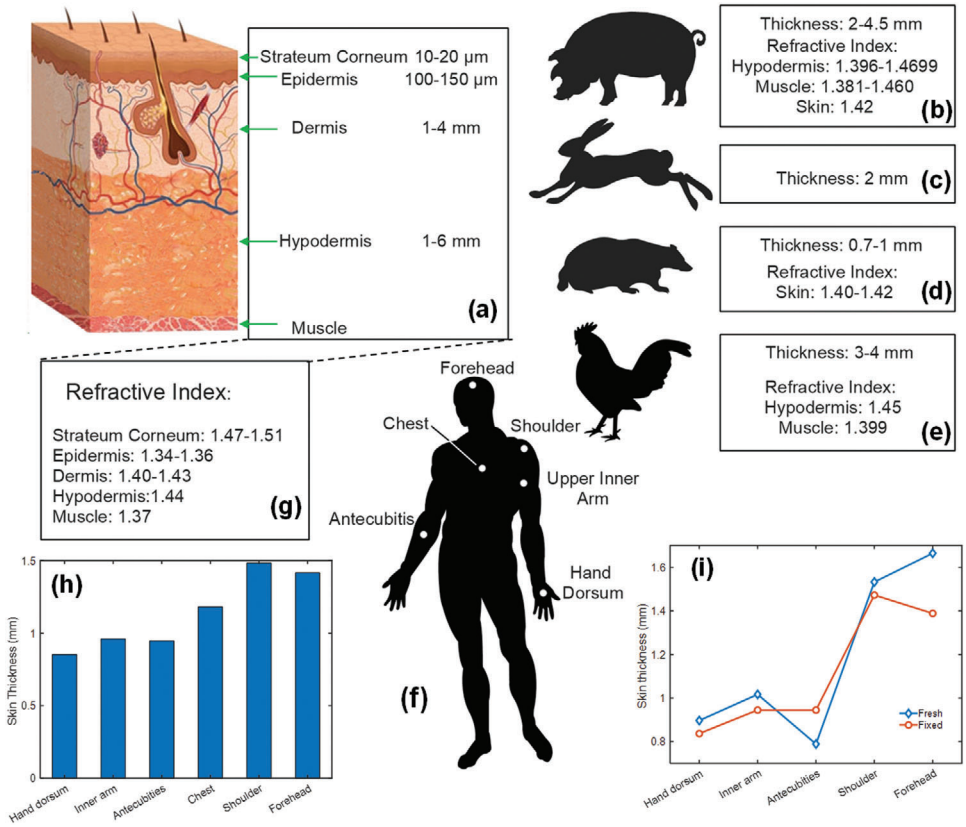

Figure 8. a) The structure of human skins. As a multi-layer structure, the skins are composed of four parts: strateum corneum, epidermis, dermis, and hypodermis. The relative thickness of each layer is shown. b) The thickness and refractive index of pork skin.[86] c) The thickness of the rabbit skin which applied in previous works.[86] d) The thickness and refractive index of rat skin in previous works.[86] e) The thickness and refractive index of chicken skin in previous works.[86] f) The skins in different locations of the human body which are applied in previous work.[91] g) The refractive indexes of the different skin layers in the skin structure, which are based on a previous study.[119] h) The skin thickness according to panel (f).[91] i) The thickness of fresh and fixed skins according to different locations of the human body.[91]

with different optical properties. The skin layers are the stratum corneum, epidermis and dermis.[134]

Due to its similarity with human tissue, animal tissue is commonly used for in vivo testing of implantable PV cells. For example, the thickness of porcine is between 2 mm to 4.5 mm, and its refractive index is around 1.42, as shown in **Figure 8**a. Rabbit tissue has also been used in the literature, and the PV implantation depth was around 2 mm as in Figure 8b.[86] Since the application is intraocular, the refractive index of the tissue was not considered. Other skin types that have been tested include rat skin. Its thickness ranges from 0.7 to 1 mm,[119] and its refractive index is between 1.40 and 1.42, as shown in Figure 8d.[119] Chicken muscle also has similar properties to human muscle. The thickness of chicken skin or muscles applied in the previous study is from 3 to 4 mm in Figure 8e.[119] Relatively, the hypodermis and muscle refractive index are 1.45 and 1.399, respectively.

As previously mentioned, human skin is a complex heterogeneous medium. Therefore, greater light attenuation takes place with depth due to the random spatial distribution of blood, chromophores and pigments within skin tissue. Moreover, different skin types will attenuate light differently due to age, ethnic group, site of body, and gender.[56] Generally, skin is composed of four main visible layers from the top surface: the blood-free epidermis (100–150 μm thick), vascularized dermis (1–4 mm thick), and subcutaneous fat layer (hypodermis or adipose tissue) (1–6 mm thick various with different body parts).

The thicknesses and refractive indices of different skin types are shown in Figure 8a,g. Furthermore, the epidermis can be divided into two parts: the living part and the non-living part.[119] The top layer is the strateum corneum, which is known as the non-living epidermis (dead squamous cells only) and its thickness varies from 10 to 20 μm. The strateum corneum is highly keratinized with 20% lipid content, 60% protein content and 20% water content. The refractive index of strateum corneum ranges between 1.47 and 1.51.[119] The living epidermis consists of mostly pigments (most of them are melanin) compared with the other tissues. The content of melanosome, a particle used to produce melanin, varies from 1.3% (lightly pigmented) to 43% (highly pigmented).[119] This pigment content is distinctive from individual to individual, and higher pigment can result in higher melanin absorptions as **Figure 9**a.

Dermis and epidermis are separated by a basal lamina, and dermis is known as the main absorber of visible light according to the blood haemoglobin, beta-carotene, and bilirubin in the layer. The absorption of IR light is related to the water content in the dermis.[119] The absorption coefficients of different

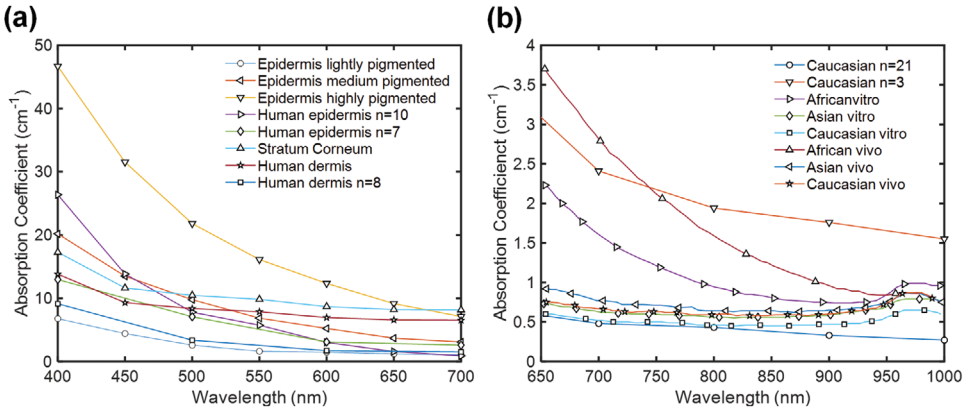

Figure 9. a) shows the absorption coefficient of human skin according to different wavelengths of the incident light. In the work of Bashkatov et al. 2011,[119] the skin properties in different locations from strateum to dermis are reported. b) The absorption coefficient according to the different light spectra. The three ethnic groups including Caucasian, Asian, and African are analyzed in ref. [119]

skin layers are shown in Figure 9a, and the absorptions in the visible spectral range are much higher than those in the IR region. For instance, the absorption coefficient of highly pigmented epidermis is around 50 cm^{-1} at 650 nm while it is 10 cm^{-1} at 700 nm. The skin properties are also different from different ethnic groups, which is shown in Figure 9b. The absorption coefficients of the Caucasian (<1 cm^{-1}) and the Asian skins (<1 cm^{-1}) are much smaller than that of African skins (>3.5 cm^{-1}) when using 650 nm visible light. All the absorption coefficients of these skins in three different ethnics saturates to 1 cm^{-1} when using 1000 nm NIR light. The optical absorptions in in vitro test is smaller than those of in vivo test as well, and the water content in the skins causes more absorptions as well. For example, when using 650 nm visible light, the African skin has different absorption coefficient in vitro (2.2 cm^{-1}) and in vivo (3.7 cm^{-1}). Based on the curves in Figure 7a,b, the NIR light shows the advantages:1. Less attenuations compared with lower wavelength. 2. Majority of types of skins including in vivo, in vitro, different ethnics and different layers converge to 1 cm^{-1}.

3.5. Biocompatibility

As most of the implantable PV cells are made from silicon, it is quite necessary to investigate material degradation. The hydrolysis process of silicon materials can be simply interpreted as the reaction between water vapor and silicon producing silicic acid.[97] Plenty of factors affect the dissolution rates of c-Si, μc-Si and a-Si, such as pH level and temperatures.[97] The silicon dissolution takes place when the silicon PV cell is implanted, which ranges from 1 nm per day to 1 nm s^{-1} relying on the pH levels in the ambient. The dissolution of different silicon structures at 37 Celsius in the butter solution is shown in **Figure 10**a–c.[97,135,136] It is noticed that the polysilicon and a-Si have a slower dissolution rate than that of the c-Si when comparing the slope in Figure 3a–c. When the pH level is less than 7, the a-Si (>20 nm dissolution in 15 days) will slightly dissolute faster than polysilicon (<20 nm dissolution in 15 days). Moreover, silicon dissolution is also influenced by the doping profile in the layers.[97]

In vivo and in vitro testing is necessary to determine the biocompatibility and cytotoxicity of the implants. Due to the similarity with human skin, testing is largely performed in chicken, rats, pigs and rabbits.[80,86,89,95] There has also been testing of implantable PV cells in different skin locations of the body.[91] Moreover, an ultrathin monocrystalline silicon solar cell array that includes the active layers, electrodes, interconnections and fully biocompatible encapsulation layers was demonstrated in.[104] In their study, the array was tested for seven days in vivo in a hairless rat. Cytotoxicity testing proved that between 89% to 91% of cells were living after seven days, which means that there is minimal toxic effects, as shown in Figure 10e. Throughout the experiment, the number of dead cells (9–18) is significantly lower than the number of living cells (around 85–175), as shown in Figure 10f, which indicates that there is good biocompatibility. Further long-term testing in different skin locations is necessary to determine the performance of these cells and to appreciate the possible side effects of these implantable devices on the wearer.[2]

In 2015, polysilicon thin-film PV cells were implanted in a mouse.[97,136] The results show the fibroblast cell viability was over 95% after seven days the similar results of a-Si, SiGe, Ge, and mono-crystalline were also shown in Figure 10d.[136] In the research of Song 2016, the survivability of the HDF cells extracted from the IPV device is similar to that from the biocompatible materials, such as encapsulation-only or glass (Figure 10g). The survivability degraded massively when higher concentration from toxic ZDEC-PU film (over 25%).[89]

Long-term in vivo or in vitro is a key factor to test the duration of implantable devices under the skin. Only a few implantable PV cells passed these tests, which are shown in Figure 10h. The longest lifespan is achieved in a rabbit in 2004, and the cell survived over 7 months after implanted in retinal.[86] Despite the previous retinal sample, the rest lifespans of PV cells are less than 4 months according to the device failure or manually stop the measuring process. This problem can be caused by the issue mentioned in Section 3.4: no evidence has pointed out that the polymer encapsulation can protect the integrated circuit in the long term.

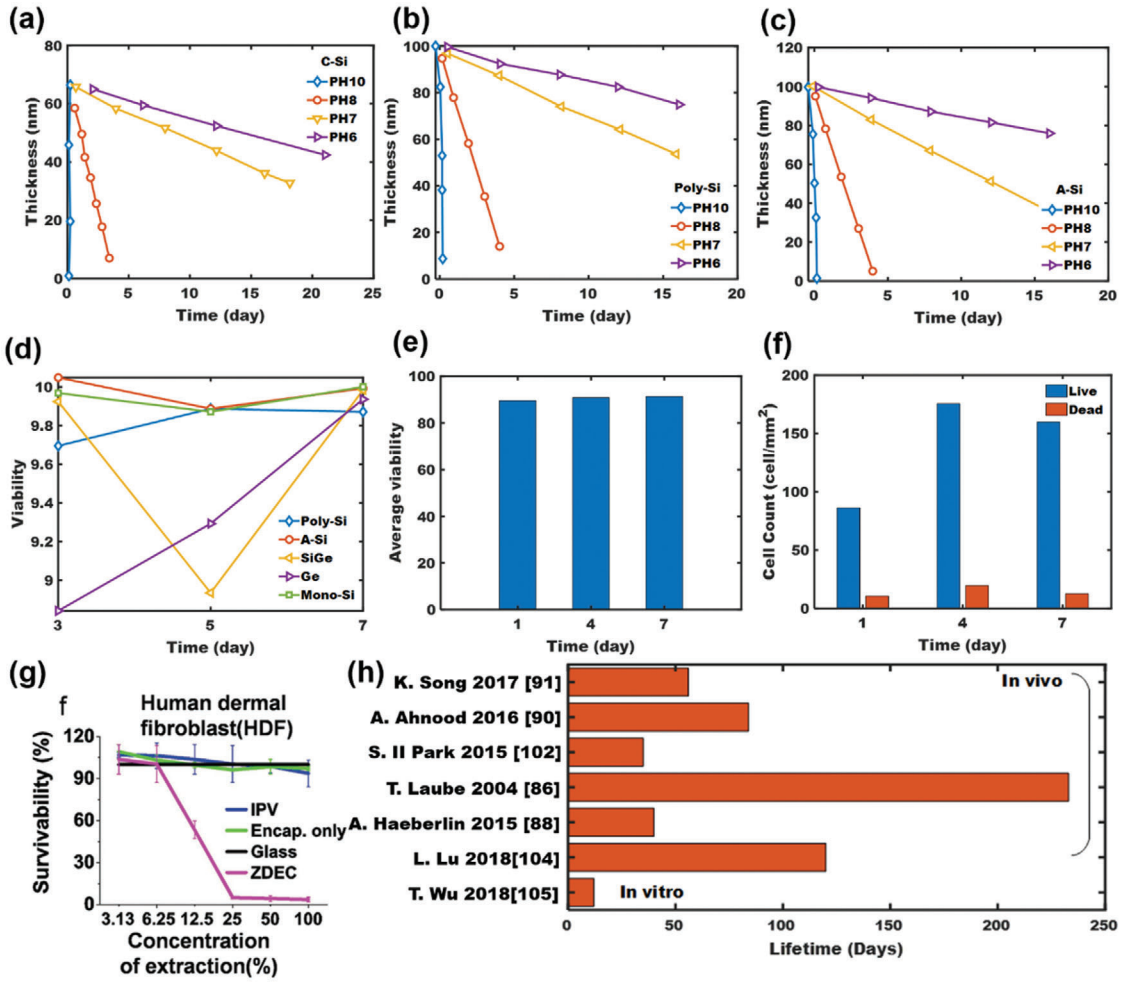

Figure 10. a) The dissolution of crystalline silicon according to different pH levels at 37 °C, where lines are theoretical values and dots are experimental values. b) The relative dissolution of poly silicon and c) a-Si. d) The viability of semiconductor materials which are normally used to fabricate implantable photovoltaic cells. e) The viability of an implanted PV cells implemented.[92] f) The number of dead cells and living cells after PV cell was implanted.[92] g) The survivability of the human dermal fibroblast cells after 24 h, extracted from implantable photovoltaic (IPV) device encapsulation layer only, glass, and 0.1% zinc diethyldithiocarbamate (ZDEC) polyurethane (PU) film. h) The lifespan of the implantable device powered by photovoltaic cells in vivo and in vitro. Reproduced with permission.[89] Copyright 2020, IEEE and Copyright Clearance Center.

4. Challenges and Future Development

PV energy harvesting is a mature technology that can be used for implantable electronic devices.[94] However, there are a few challenges. First, semiconductor PV cells are rigid and expensive. Organic PV cells can be an alternative to these semiconductor technologies, provided that the efficiency and lifetime can be improved. Typically, organic materials are much cheaper than semiconductors and PV cell can be fabricated using solution-based techniques in room temperature conditions. Second, internal body heat reduces the efficiency of PV cells. Third, people typically spend more time indoors, which means that these devices will rely on indoor light for energy harvesting purposes. Thus, the amount of harvestable energy is severely compromised. In 2015, Haeberlin et al. tested the indoor performance (incident power density of 4 W m^{-2} at a distance of 2 m from a closed window without direct sunlight exposure) of the implantable PV cell and reported a 4 μW cm^{-2} (1% of efficiency) output power in in vivo test (female pork).[87,88] In 2018, Wu et al. used a 24 W fluorescent lamp to test the PV cells (64×37 mm^2) in indoor conditions in vitro for pork skin. Only 120 μW of power was harvested, which was sufficient to supply the low-power consuming biomedical sensors.[105] Consequently, implantable PV cells have to be optimized for this type of lighting. Finally, even most of encapsulations for implantable PV cells are with high optical transmittance, only polymer encapsulation can provide high flexibility and comfortability, but more supportive evidence is required to show their biocompatibility.

5. Conclusions and Recommendations

In summary, the factors which influence the performances of different power harvesters. With the consideration in system level, implantable PV cells are more promising in harvested energy, smaller size, less complexity in power conversion, and

flexible configurations. Considering the electrical performance, the implantable PV cells are also advantageous for stable output voltage and hundreds of mA current. With the development of two decades, the great achievement has been made not only in the off-chip instrument but on-chip measurement or even in vitro and in vivo biocompatibility tests. The implantable PV energy harvesting system is finalized with device fabrication, on-chip power management circuitry and encapsulations. The polymer encapsulation and hermetic package are applied to protect the PV cell from subcutaneous fluids. The mono-crystalline silicon is mostly used in the implantable PV cell fabrication, while the polysilicon and a-Si are advantageous for slower dissolution. Without encapsulation, the bio-performance of silicon is much better than the other materials. The a-Si is promising with the best performance in device viability, followed by mono-Si and polysilicon. Nevertheless, the electrical output characteristic of mono-silicon is much better than a-Si, and the polysilicon is advantageous in material cost reduction. Turning the point to the package and encapsulation, the cell viability of previous studies shows that the implantable PV cell with encapsulation is highly biocompatible. Two types of encapsulation structure can be used, which are hermetic package and polymer encapsulation. The hermetic structure is proposed with long-term stability in in vivo test, while there is lack of evidence to show the stability of polymer encapsulation in the implantable applications. It must be emphasized that the comfortability and flexibility of the polymer encapsulation is much better than the hermetic, while the hermetic structure provide the better protection for the devices. The other factors such as light source and optical skin loss can also affect the performance of PV cell. The NIR light is confirmed as a nice input power source of the implantable PV cells if the heating problem can be solved. The human tissue various with different ethnic group, different location, different age and even different part of body in same person is summarized. The previous research shows the African skin will cause more losses than that of Caucasian and Asian. Moreover, it is also shown that the PV cell in dermis can harvest move power than that in hypodermis, while the cells in hypodermis can provide more stable energy. The hand skin is one of the best parts to implant PV cells because of the lower thickness. In popular believe, the in vivo test of human implantation is far away from the PV cells now. The best alternative subject is pork skin because of the similar thickness and skin properties. In conclusion, the implantable PV cell is advantageous in supplying the sufficient power within small area compared with the other power harvesting techniques. The circuitry of the PV cell is not as complex as the other AC source. However, there are still some constrains of implantable PV cells: Low feasibility and intensity of the light, rigid and expensive materials, penetration depth for PV cell to implant in surface area of tissue and still need investigation on long term performance after implantation.

Based on the literature review in this article, it is clear that there has been plenty of interest in using PV cells for powering implantable electronic devices. These cells have their limitations and advantages. Their main advantage is the large power density that can be generated. Their main limitation is the difficulty in harnessing light due to tissue losses. However, since all energy harvesters have their limitations, we believe that using a hybrid harvester can help remedy this problem. Hybrid energy harvesters are capable of scavenging energy from multiple sources, thereby offsetting any limitations caused by the unavailability of energy from one source. In this case, the system is guaranteed to receive energy in case one or more energy sources are unavailable.

Acknowledgements

This work was supported by grant EP/R511705/1 from EPSRC, UK, and the European Union's Horizon 2020 Hybrid Enhanced Regenerative Medicine Systems (HERMES) project (GA n. 824164).

Conflict of Interest

The authors declare no conflict of interest.

Keywords

energy harvesting, implantable devices, photovoltaics

Received: May 8, 2020
Revised: July 9, 2020
Published online: July 29, 2020

[1] R. Das, F. Moradi, H. Heidari, *IEEE Trans. Biomed. Circuits Syst.* **2020**, *14*, 343.
[2] B. Shi, Z. Li, Y. Fan, *Adv. Mater.* **2018**, *30*, 1801511.
[3] X.-Y. Lang, H.-Y. Fu, C. Hou, G.-F. Han, P. Yang, Y.-B. Liu, Q. Jiang, *Nat. Commun.* **2013**, *4*, 1.
[4] a) D. J. Ecker, R. Sampath, C. Massire, L. B. Blyn, T. A. Hall, M. W. Eshoo, S. A. Hofstadler, *Nat. Rev. Microbiol.* **2008**, *6*, 553; b) J. Arlett, E. Myers, M. Roukes, *Nat. Nanotechnol.* **2011**, *6*, 203.
[5] a) A.-H. Cavusoglu, X. Chen, P. Gentine, O. Sahin, *Nat. Commun.* **2017**, *8*, 617; b) M. Parvez Mahmud, N. Huda, S. H. Farjana, M. Asadnia, C. Lang, *Adv. Energy Mater.* **2018**, *8*, 1701210; c) S. Gong, W. Cheng, *Adv. Energy Mater.* **2017**, *7*, 1700648.
[6] Q. Zheng, B. Shi, F. Fan, X. Wang, L. Yan, W. Yuan, S. Wang, H. Liu, Z. Li, Z. L. Wang, *Adv. Mater.* **2014**, *26*, 5851.
[7] Y. Jiang, M.-K. Law, P.-I. Mak, R. P. Martins, *IEEE J. Solid-State Circuits* **2018**, *53*, 3455.
[8] X. Liu, L. Huang, K. Ravichandran, E. Sánchez-Sinencio, *IEEE J. Solid-State Circuits* **2016**, *51*, 1302.
[9] J. P. DiMarco, *N. Engl. J. Med.* **2003**, *349*, 1836.
[10] F. Rezai, *Oral Surg., Oral Med., Oral Pathol.* **1977**, *44*, 662.
[11] S. Park, X. Guan, Y. Kim, F. X. Creighton, E. Wei, I. Kymissis, H. H. Nakajima, E. S. Olson, *Trends Hear.* **2018**, *22*, 2331216518774450.
[12] a) G. Clark, in *Speech Processing in the Auditory System*, Vol. *18*, Springer, New York **2004**, p. 422; b) J. Žák, Z. Hadaš, D. Dušek, J. Pekárek, V. Svatoš, L. Janák, J. Prášek, *Mechatronics* **2015**, *31*, 30.
[13] a) P. Song, S. Kuang, N. Panwar, G. Yang, D. J. H. Tng, S. C. Tjin, W. J. Ng, M. B. A. Majid, G. Zhu, K. T. Yong, *Adv. Mater.* **2017**, *29*, 1605668; b) R. Riahi, A. Tamayol, S. A. M. Shaegh, A. M. Ghaemmaghami, M. R. Dokmeci, A. Khademhosseini, *Curr. Opin. Chem. Eng.* **2015**, *7*, 101.
[14] L. W. Kleiner, J. C. Wright, Y. Wang, *J. Controlled Release* **2014**, *181*, 1.
[15] a) T. Tokuda, T. Ishizu, W. Nattakarn, M. Haruta, T. Noda, K. Sasagawa, M. Sawan, J. Ohta, *AIP Adv.* **2018**, *8*, 045018; b) K. Stingl, K. U. Bartz-Schmidt, D. Besch, A. Braun, A. Bruckmann, F. Gekeler, U. Greppmaier, S. Hipp, G. Hörtdörfer, C. Kernstock, A. Koitschev,

A. Kusnyerik, H. Sachs, A. Schatz, K. T. Stingl, T. Peters, B. Wilhelm, E. Zrenner, *Proc. Royal Soc. B: Biol. Sci.* **2013**, *280*, 20130077.
[16] J. D. Weiland, W. Liu, M. S. Humayun, *Annu. Rev. Biomed. Eng.* **2005**, *7*, 361.
[17] G.-T. Hwang, M. Byun, C. K. Jeong, K. J. Lee, *Adv. Healthcare Mater.* **2015**, *4*, 646.
[18] K. Agarwal, R. Jegadeesan, Y.-X. Guo, N. V. Thakor, *IEEE Rev. Biomed. Eng.* **2017**, *10*, 136.
[19] a) J. Zhao, R. Ghannam, M. K. Law, M. A. Imran, H. Heidari, *IEEE J. Elect. RF Microwaves Med. Biol.* **2019**, *4*, 148; b) L. Bereuter, S. Williner, F. Pianezzi, B. Bissig, S. Buecheler, J. Burger, R. Vogel, A. Zurbuchen, A. Häberlin, *Ann. Biomed. Eng.* **2017**, *45*, 1172.
[20] S. Abdellatif, K. Kirah, R. Ghannam, A. Khalil, W. Anis, *Appl. Opt.* **2015**, *54*, 5534.
[21] a) S. O. Abdellatif, K. Kirah, R. Ghannam, A. Khalil, W. Anis, *Int. J. Recent Contrib. Eng. Sci. IT* **2016**, *4*, 63; b) S. Abdellatif, R. Ghannam, A. Khalil, *Appl. Opt.* **2014**, *53*, 3294.
[22] J. Li, J. Seo, I. Kymissis, M. Seok, *IEEE J. Solid-State Circuits* **2017**, *52*, 2550.
[23] K. Htet, R. Ghannam, Q. Abbasi, H. Heidari, *IEEE Access* **2018**, *6*, 42156.
[24] K. Oo Htet, R. Ghannam, Q. H. Abbasi, H. Heidari, *IEEE Access* **2018**, *6*, 42156
[25] M. Ashraf, N. Masoumi, *IEEE Trans. Very Large Scale Integr. Syst.* **2016**, *24*, 26.
[26] A. Cadei, A. Dionisi, E. Sardini, M. Serpelloni, *Meas. Sci. Technol.* **2013**, *25*, 012003.
[27] T. Tokuda, T. Ishizu, W. Nattakarn, M. Haruta, T. Noda, K. Sasagawa, M. Sawan, J. Ohta, *AIP Adv.* **2018**, *8*, 045018.
[28] A. P. Chandrakasan, N. Verma, D. C. Daly, *Annu. Rev. Biomed. Eng.* **2008**, *10*, 247.
[29] V. Nabaei, R. Chandrawati, H. Heidari, *Biosens. Bioelectron.* **2018**, *103*, 69.
[30] X. Liang, R. Ghannam, H. Heidari, *IEEE Sensors Journal* **2019**, *19*, 1082.
[31] X. Wei, J. Liu, *Front. Energy Power Eng. China* **2008**, *2*, 1.
[32] H. Zhang, X.-S. Zhang, X. Cheng, Y. Liu, M. Han, X. Xue, S. Wang, F. Yang, S. A. S, H. Zhang, Z. Xu, *Nano Energy* **2015**, *12*, 296.
[33] a) C. Fernandez, O. Garcia, J. Cobos, J. Uceda, presented at IEEE 34th Annual Power Electronics Specialist Conf., PESC'03, Acapulco, Mexico, June **2003**; b) I. Hochmair, P. Nopp, C. Jolly, M. Schmidt, H. Schößer, C. Garnham, I. Anderson, *Trends Amplif.* **2006**, *10*, 201; c) J. F. Patrick, P. A. Busby, P. J. Gibson, *Trends Amplif.* **2006**, *10*, 175.
[34] M. Gross, R. Buss, K. Kohler, J. Schaub, D. Jager, presented at the First Joint BMES/EMBS Conf. 1999 IEEE Engineering in Medicine and Biology 21st Annual Conf. and the 1999 Annual Fall Meeting of the Biomedical Engineering Society, Atlanta, GA, October **1999**.
[35] L. S. Wong, S. Hossain, A. Ta, J. Edvinsson, D. H. Rivas, H. Naas, *IEEE J. Solid-State Circuits* **2004**, *39*, 2446.
[36] F. V. Y. Tjong, V. Y. Reddy, *Circulation* **2017**, *135*, 1458.
[37] R.-D. Battmer, G. M. O'donoghue, T. Lenarz, *Ear Hear.* **2007**, *28*, 95S.
[38] F.-G. Zeng, S. Rebscher, W. Harrison, X. Sun, H. Feng, *IEEE Rev. Biomed. Eng.* **2008**, *1*, 115.
[39] A. Björklund, U. Stenevi, *Annu. Rev. Neurosci.* **1984**, *7*, 279.
[40] M. S. Humayun, L. C. O. de Koo, *Retinal Prosthesis: A Clinical Guide to Successful Implementation*, Springer, New York **2018**.
[41] P. J. Blackshear, F. Dorman, P. Blackshear, R. Varco, H. Buchwald, *Surg., Gynecol. Obstet.* **1972**, *134*, 51.
[42] T. Hehn, Y. Manoli, in *CMOS Circuits for Piezoelectric Energy Harvesters*, Springer, Berlin **2015**, pp. 21–40.
[43] W. Heimisch, S. Hagl, K. Gebhardt, N. Mendler, H. Meisner, in *Physics in Medicine and Biology*, Vol. *25*, No. 5, IOP Publishing Ltd, Bristol, England **1980**.
[44] A. Khaligh, P. Zeng, C. Zheng, *IEEE Trans. Ind. Electron.* **2009**, *57*, 850.
[45] A. Khan, Z. Abas, H. S. Kim, I.-K. Oh, *Smart Mater. Struct.* **2016**, *25*, 053002.
[46] Y. Yu, H. Sun, H. Orbay, F. Chen, C. G. England, W. Cai, X. Wang, *Nano Energy* **2016**, *27*, 275.
[47] X. Cheng, X. Xue, Y. Ma, M. Han, W. Zhang, Z. Xu, H. Zhang, H. Zhang, *Nano Energy* **2016**, *22*, 453.
[48] Q. Shi, T. Wang, C. Lee, *Sci. Rep.* **2016**, *6*, 24946.
[49] C. Dagdeviren, B. D. Yang, Y. Su, P. L. Tran, P. Joe, E. Anderson, J. Xia, V. Doraiswamy, B. Dehdashti, X. Feng, *Proc. Natl. Acad. Sci. USA* **2014**, *111*, 1927.
[50] S. Ozeri, D. Shmilovitz, S. Singer, C.-C. Wang, *Ultrasonics* **2010**, *50*, 666.
[51] J. Rao, G. Richter, E. Weidlich, M. Wenzel, *Biomed. Eng.* **1974**, *9*, 98.
[52] A. A. Babadi, S. Bagheri, S. B. A. Hamid, *Biosens. Bioelectron.* **2016**, *79*, 850.
[53] M. Zhou, L. Deng, D. Wen, L. Shang, L. Jin, S. Dong, *Biosens. Bioelectron.* **2009**, *24*, 2904.
[54] J. Y. Lee, H. Y. Shin, S. W. Kang, C. Park, S. W. Kim, *Biosens. Bioelectron.* **2011**, *26*, 2685.
[55] J. Katic, S. Rodriguez, A. Rusu, *IEEE Trans. Power Electron.* **2017**, *33*, 4125.
[56] Y. Tan, W. Deng, B. Ge, Q. Xie, J. Huang, S. Yao, *Biosens. Bioelectron.* **2009**, *24*, 2225.
[57] A. Cuadras, M. Gasulla, V. Ferrari, *Sens. Actuators, A* **2010**, *158*, 132.
[58] M. Rudnicki, R. Chesworth, L. Harmison, *Trans. Am. Nucl. Soc.* **1970**, *13*, 503.
[59] S. Sedky, A. Kamal, M. Yomn, H. Bakr, R. Ghannam, V. Leonov, P. Fiorini, presented at TRANSDUCERS 2009—Int. Solid-State Sensors, Actuators and Microsystems Conf., Denver, CO, June **2009**.
[60] E.-J. Yoon, J.-T. Park, C.-G. Yu, *Front. Inf. Technol. Electron. Eng.* **2018**, *19*, 285.
[61] G. Zhang, M. Li, H. Li, Q. Wang, S. Jiang, *Energy Technol.* **2018**, *6*, 791.
[62] W. Holcomb, W. Glenn, G. Sato, *Med. Biol. Eng.* **1969**, *7*, 493.
[63] L.-G. Tran, H.-K. Cha, W.-T. Park, *Micro Nano Syst. Lett.* **2017**, *5*, 14.
[64] S. Li, C. C. Mi, *IEEE J. Emerging Sel. Topics Power Electron.* **2015**, *3*, 4.
[65] D. A. Borton, M. Yin, J. Aceros, A. Nurmikko, *J. Neural Eng.* **2013**, *10*, 026010.
[66] T.-i. Kim, J. G. McCall, Y. H. Jung, X. Huang, E. R. Siuda, Y. Li, J. Song, Y. M. Song, H. A. Pao, R.-H. Kim, *Science* **2013**, *340*, 211.
[67] C. T. Wentz, J. G. Bernstein, P. Monahan, A. Guerra, A. Rodriguez, E. S. Boyden, *J. Neural Eng.* **2011**, *8*, 046021.
[68] S. Radiom, M. Baghaei-Nejad, K. Aghdam, G. A. Vandenbosch, L.-R. Zheng, G. G. Gielen, *IEEE J. Solid-State Circuits* **2010**, *45*, 1746.
[69] Y. Shih, T. Shen, B. P. Otis, *IEEE J. Solid-State Circuits* **2011**, *46*, 2592.
[70] C. Liu, Y. Zhang, X. Liu, *IEEE Antennas Wireless Propag. Lett.* **2018**, *17*, 373.
[71] M. H. Ouda, M. Arsalan, L. Marnat, A. Shamim, K. N. Salama, *IEEE Trans. Microwave Theory Tech.* **2013**, *61*, 2177.
[72] R. Ghannam, P. V. Klaine, M. Imran, in *Solar Photovoltaic Power Plants*, Springer, New York **2019**, p. 121.
[73] X. Li, N. P. Hylton, V. Giannini, K. H. Lee, N. J. Ekins-Daukes, S. A. Maier, *Prog. Photovoltaics* **2013**, *21*, 109.
[74] S. Gong, W. Cheng, *Adv. Energy Mater.* **2017**, *7*, 1700648.
[75] J.-F. Chen, C.-L. Chun, Y. Hung, Jr., in *2015 Int. Symp. on Next-Generation Electronics*, IEEE, Piscataway, NJ **2015**, p. 1.
[76] J. Charthad, M. J. Weber, T. C. Chang, A. Arbabian, *IEEE J. Solid-State Circuits* **2015**, *50*, 1741.
[77] M. Schormans, V. Valente, A. Demosthenous, *IEEE Trans. Biomed. Circuits Syst.* **2018**, *12*, 1112.
[78] Q. Zheng, H. Zhang, B. Shi, X. Xue, Z. Liu, Y. Jin, Y. Ma, Y. Zou, X. Wang, Z. An, W. Tang, W. Zhang, F. Yang, Y. Liu, X. Lang, Z. Xu, Z. Li, Z. L. Wang, *ACS Nano* **2016**, *10*, 6510.

[79] a) K. Shoji, Y. Akiyama, M. Suzuki, N. Nakamura, H. Ohno, K. Morishima, *Biosens. Bioelectron.* **2016**, *78*, 390; b) J. Schwefel, R. E. Ritzmann, I. N. Lee, A. Pollack, W. Weeman, S. Garverick, M. Willis, M. Rasmussen, D. Scherson, *J. Electrochem. Soc.* **2015**, *161*, H3113; c) K. MacVittie, J. Halámek, L. Halámková, M. Southcott, W. D. Jemison, R. Lobel, E. Katz, *Energy Environ. Sci.* **2012**, *6*, 81; d) L. Halámková, J. Halámek, V. Bocharova, A. Szczupak, L. Alfonta, E. Katz, *J. Am. Chem. Soc.* **2012**, *134*, 5040.
[80] S. Ayazian, V. A. Akhavan, E. Soenen, A. Hassibi, *IEEE Trans. Biomed. Circuits Syst.* **2012**, *6*, 336.
[81] Z. Chen, M.-K. Law, P.-I. Mak, R. P. Martins, *IEEE Trans. Biomed. Circuits Syst.* **2017**, *11*, 44.
[82] a) M. A. Green, Y. Hishikawa, E. D. Dunlop, D. H. Levi, J. Hohl-Ebinger, A. W. Y. Ho-Baillie, *Prog. Photovoltaics* **2018**, *26*, 3; b) M. A. Green, Y. Hishikawa, W. Warta, E. D. Dunlop, D. H. Levi, J. Hohl-Ebinger, A. W. Ho-Baillie, *Prog. Photovoltaics* **2017**, *26*, 3.
[83] M. K. Law, A. Bermak, *IEEE Electron Device Lett.* **2010**, *31*, 1425.
[84] G. Simone, D. Di Carlo Rasi, X. de Vries, G. H. Heintges, S. C. Meskers, R. A. Janssen, G. H. Gelinck, *Adv. Mater.* **2018**, *30*, 1804678.
[85] A. V. Dan Tchin-Iou, B. G. Min, *Int. J. Artif. Organs* **1999**, *22*, 823.
[86] T. Laube, C. Brockmann, R. Buß, C. Lau, K. Höck, N. Stawski, T. Stieglitz, H. A. Richter, H. Schilling, *Graefe's Arch. Clin. Exp. Ophthalmol.* **2004**, *242*, 661.
[87] A. Haeberlin, A. Zurbuchen, J. Schaerer, J. Wagner, S. Walpen, C. Huber, H. Haeberlin, J. Fuhrer, R. Vogel, *EP Europace* **2014**, *16*, 1534.
[88] A. Haeberlin, A. Zurbuchen, S. Walpen, J. Schaerer, T. Niederhauser, C. Huber, H. Tanner, H. Servatius, J. Seiler, H. Haeberlin, J. Fuhrer, R. Vogel, *Heart Rhythm* **2015**, *12*, 1317.
[89] K. Song, J. H. Han, T. Lim, N. Kim, S. Shin, J. Kim, H. Choo, S. Jeong, Y.-C. Kim, Z. L. Wang, J. Lee, *Adv. Healthcare Mater.* **2016**, *5*, 1572.
[90] A. Ahnood, K. E. Fox, N. V. Apollo, A. Lohrmann, D. J. Garrett, D. A. X. Nayagam, T. Karle, A. Stacey, K. M. Abberton, W. A. Morrison, A. Blakers, S. Prawer, *Biosens. Bioelectron.* **2016**, *77*, 589.
[91] K. Song, J. H. Han, H. C. Yang, K. I. Nam, J. Lee, *Biosens. Bioelectron.* **2017**, *92*, 364.
[92] C. Yan, P. S. Lee, *Small* **2014**, *10*, 3443.
[93] E. Płaczek-Popko, *Opto-Electron. Rev.* **2017**, *25*, 55.
[94] M. A. Hannan, S. Mutashar, S. A. Samad, A. Hussain, *Biomed. Eng. Online* **2014**, *13*, 79.
[95] E. Moon, D. Blaauw, J. D. Phillips, *IEEE Trans. Electron. Devices* **2017**, *64*, 2432.
[96] P. G. V. Sampaio, M. O. A. González, *Renewable Sustainable Energy Rev.* **2017**, *74*, 590.
[97] X. Sheng, S. Wang, L. Yin, in *Advances in Silicon Solar Cells*, Springer, New York **2018**, p. 161.
[98] G. Bo, L. Ren, X. Xu, Y. Du, S. Dou, *Adv. Phys.: X* **2018**, *3*, 1446359.
[99] S. Sze, G. Gibbons, *Appl. Phys. Lett.* **1966**, *8*, 111.
[100] Y. Hung, Jr., M.-S. Cai, J.-F. Chen, H.-W. Su, P.-C. Jen, P. Chen, C.-C. Shih, T.-C. Chang, *IEEE J. Photovoltaics* **2018**, *8*, 342.
[101] Y. Hung, Jr., T.-Y. Chuang, C.-L. Chun, M.-S. Cai, H.-W. Su, S.-L. Lee, *IEEE Trans. Electron. Devices* **2014**, *61*, 4019.
[102] S. Il Park, G. Shin, A. Banks, J. G. McCall, E. R. Siuda, M. J. Schmidt, H. U. Chung, K. N. Noh, J. G.-H. Mun, J. Rhodes, M. R. Bruchas, J. A. Rogers, *J. Neural Eng.* **2015**, *12*, 056002.
[103] E. Moon, D. Blaauw, J. D. Phillips, *IEEE Trans. Electron Devices* **2017**, *64*, 15.
[104] L. Lu, Z. Yang, K. Meacham, C. Cvetkovic, E. A. Corbin, A. Vazquez-Guardado, M. Xue, L. Yin, J. Boroumand, G. Pakeltis, T. Sang, K. J. Yu, D. Chanda, R. Bashir, R. W. Gereau, X. Sheng, J. A. Rogers, *Adv. Energy Mater.* **2018**, *8*, 1703035.
[105] T. Wu, J.-M. Redouté, M. R. Yuce, *IEEE Access* **2018**, *6*, 35801.
[106] Y. Arima, M. Ehara, *IEICE Elect. Exp.* **2006**, *3*, 287.
[107] K. Shen, M. M. Maharbiz, presented at the 9th Int. IEEE/EMBS Conf. on Neural Engineering (NER), San Francisco, CA, March **2019**.
[108] S.-H. Ahn, J. Jeong, S. J. Kim, *Micromachines* **2019**, *10*, 508.
[109] A. Vanhoestenberghe, N. Donaldson, *J. Neural Eng.* **2013**, *10*, 031002.
[110] M. R. Querry, *Optical Constants*, Missouri University, Kansas City, MO **1985**.
[111] D. L. Wood, K. Nassau, T. Kometani, D. Nash, *Appl. Opt.* **1990**, *29*, 604.
[112] T. T. S. Popova, V. Vorobev, *Opt. Spectrosc.* **1972**, *33*, 444.
[113] G. Ghosh, *Opt. Commun.* **1999**, *163*, 95.
[114] L. V. Rodríguez-de Marcos, J. I. Larruquert, J. A. Méndez, J. A. Aznárez, *Opt. Mater. Express* **2016**, *6*, 3622.
[115] H. R. Philip, E. A. Taft, *Phys. Rev.* **1964**, *136*, A1445.
[116] M. R. Vogt, H. Holst, H. Schulte-Huxel, S. Blankemeyer, R. Witteck, D. Hinken, M. Winter, B. Min, C. Schinke, I. Ahrens, *Energy Procedia* **2016**, *92*, 523.
[117] T. P. Otanicar, P. E. Phelan, J. S. Golden, *Sol. Energy* **2009**, *83*, 969.
[118] J. Li, C.-H. Wen, S. Gauza, R. Lu, S.-T. Wu, *J. Disp. Technol.* **2005**, *1*, 51.
[119] A. N. Bashkatov, E. A. Genina, V. V. Tuchin, *J. Innovative Opt. Health Sci.* **2011**, *4*, 9.
[120] R. Caldwell, H. Mandal, R. Sharma, F. Solzbacher, P. Tathireddy, L. Rieth, *J. Neural Eng.* **2017**, *14*, 046011.
[121] J. Jeong, F. Laiwalla, J. Lee, R. Ritasalo, M. Pudas, L. Larson, V. Leung, A. Nurmikko, *Adv. Funct. Mater.* **2019**, *29*, 1806440.
[122] H. Fang, J. Zhao, K. J. Yu, E. Song, A. B. Farimani, C.-H. Chiang, X. Jin, Y. Xue, D. Xu, W. Du, *Proc. Natl. Acad. Sci. USA* **2016**, *113*, 11682.
[123] a) V. Woods, M. Trumpis, B. Bent, K. Palopoli-Trojani, C.-H. Chiang, C. Wang, C. Yu, M. N. Insanally, R. C. Froemke, J. Viventi, *J. Neural Eng.* **2018**, *15*, 066024; b) K. Palopoli-Trojani, V. Woods, C.-H. Chiang, M. Trumpis, J. Viventi, presented at the 38th Annual Int. Conf. of the IEEE Engineering in Medicine and Biology Society (EMBC), Orlando, FL, August **2016**.
[124] S. W. Lee, K. S. Min, J. Jeong, J. Kim, S. J. Kim, *IEEE Trans. Biomed. Eng.* **2011**, *58*, 2255.
[125] J. H.-C. Chang, Y. Liu, Y.-C. Tai, presented at the IEEE 27th Int. Conf. on Micro Electro Mechanical Systems (MEMS), San Francisco, CA, January **2014**.
[126] H. Heidari, N. Wacker, R. Dahiya, *Appl. Phys. Rev.* **2017**, *4*, 031101.
[127] M. J. Weber, *Handbook of Optical Materials*, CRC Press, Boca Raton, FL **2018**.
[128] a) G. D. Wilk, R. M. Wallace, J. Anthony, *J. Appl. Phys.* **2001**, *89*, 5243; b) J. Choi, Y. Mao, J. Chang, *Mater. Sci. Eng., R* **2011**, *72*, 97.
[129] D. Schaubroeck, R. Verplancke, M. Cauwe, D. Cuypers, K. Baumans, M. Op de Beeck, presented at the XXXI Int. Conf. on Surface Modification Technologies (SMT31), Mons, Belgium, July **2017**.
[130] S. Popova, T. Tolstykh, V. Vorobev, *Opt. Spectrosc.* **1972**, *33*, 444.
[131] I. Dion, C. Baquey, J. Monties, *Int. J. Artif. Organs* **1993**, *16*, 623.
[132] B. Ketola, K. R. McIntosh, A. Norris, M. K. Tomalia, presented at the 23rd European Photovoltaic Solar Energy Conf., Valencia, Spain, September **2008**.
[133] S. L. Jacques, *Phys. Med. Biol.* **2013**, *58*, R37.
[134] a) P. A. Kolarsick, M. A. Kolarsick, C. Goodwin, *J. Dermatol. Nurses' Assoc.* **2011**, *3*, 203; b) M. Geerligs, *Ph.D. Thesis*, Eindhoven University of Technology, **2010**; c) R. R. Anderson, J. A. Parrish, *J. Invest. Dermatol.* **1981**, *77*, 13.
[135] S. W. Hwang, G. Park, H. Cheng, J. K. Song, S. K. Kang, L. Yin, J. H. Kim, F. G. Omenetto, Y. Huang, K. M. Lee, *Adv. Mater.* **2014**, *26*, 1992.
[136] S.-K. Kang, G. Park, K. Kim, S.-W. Hwang, H. Cheng, J. Shin, S. Chung, M. Kim, L. Yin, J. C. Lee, *ACS Appl. Mater. Interfaces* **2015**, *7*, 9297.

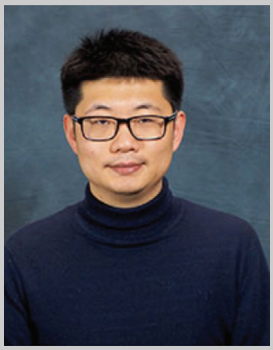

Jinwei Zhao received a B.Eng. degree in electrical and electronics engineering, University of Edinburgh, 2016 and received an M.Sc. degree in electric power, Newcastle University, UK, 2017. He has been a Ph.D. student at the University of Glasgow, since January 2018. The research interest is energy harvesting, implantable systems and photovoltaic cells. He participated in the FDCT (The Science and Technology Development Fund) funded project "High efficiency Energy Harvesting System for Biomedical Devices" and exchanged to the State Key Laboratory of Analog and Mixed-signal VLSI group (University of Macau) in 2019.

Rami Ghannam is a lecturer (assistant professor) in electronic and nanoscale engineering. Following his Ph.D. from Cambridge University in 2007, he spent the past 10 years in the field of photovoltaics. He has held previous appointments at Nortel Networks and IBM Research GmbH. He received his B.Eng. degree from King's College, as well as his DIC and M.Sc. degrees from Imperial College London. He is currently investigating the use of energy harvesters for wearable and implantable electronic devices. He is a member of the IET and a Senior Member of the IEEE.

Kaung Oo Htet was born in Yangon, Burma. He is currently doing his Ph.D. degree at the Microelectronics Lab (meLAB) at the University of Glasgow. He received his M.Phil. degree in autonomous power systems for bio devices from Newcastle University in 2016, M.Sc. (Merits) in automation and control from Newcastle University in 2013 and B.Eng. (Hons) in electronic engineering from the University of Birmingham. He also achieved his BITE award (Distinctions) and HND foundation (Merits) from Wigan and Leigh College in 2008–2009. His research interest is integrated power management system for wearable and implantable devices.

Yuchi Liu received her B.Eng. degree in electronic information engineering, University of Electronic Science and Technology of China in 2017 and received an M.Sc. degree in electrical and electronics engineering, University of Glasgow, UK, 2018. She is currently a Ph.D. student at the University of Glasgow, since February 2019. Her research interests mainly focus on wearable electronics, gesture recognition, and piezoelectric sensors.

Man-Kay Law received his B.Sc. degree in computer engineering and the Ph.D. degree in electronic and computer engineering from Hong Kong University of Science and Technology (HKUST), in 2006 and 2011, respectively. In February 2011, he joined HKUST as a visiting assistant professor. He is currently an assistant professor at the State Key Laboratory of Analog and Mixed-Signal VLSI, Faculty of Science and Technology, University of Macau, Macau, China. His research interests are on the development of ultra-low power CMOS sensing/readout circuits and energy harvesting techniques for wireless and biomedical applications.

Roy Vellaisamy is a professor of intelligent systems at the James Watt School of Engineering, University of Glasgow. He works on multidisciplinary research blending device physics with materials chemistry and electronic engineering with particular focuses on intelligent devices and systems for sensing application, wearable thermoelectrics, piezoresistive sensors, and neuromorphic devices.

Bruno Michel received a Ph.D. degree in biochemistry and computer engineering from the University of Zurich and joined IBM Research to work on scanning probe microscopy and soft lithography. He improved thermal interfaces and miniaturized convective cooling and demonstrated improved efficiency and energy re-use in datacenters, and photovoltaic thermal solar concentrators. Recently he focusses on integration of IoT and wearable devices with efforts spanning from sensing principles over efficient miniaturized compute platforms to multi-sensor data fusion and cognitive computing. He is an IEEE Fellow, a member of the US National Academy of Engineering and the IBM Academy of Technology.

Muhammad Ali Imran, Fellow IET, Senior Member IEEE, Senior Fellow HEA is a professor of wireless communication systems with research interests in self-organized networks, wireless networked control systems and the wireless sensor systems. He heads the Communications, Sensing and Imaging CSI research group at University of Glasgow. He is an affiliate professor at the University of Oklahoma, USA, and a visiting professor at 5G Innovation Centre, University of Surrey, UK.

Hadi Heidari is a senior lecturer (associate professor) in the James Watt School of Engineering at the University of Glasgow, UK. He is leading the Microelectronics Lab (meLAB) and his research includes developing microelectronics for wearable and implantable devices. He is a member of the IEEE Circuits and Systems Society Board of Governors (2018–2020), IEEE Sensors Council Member-at-Large (2020–2021), senior member of IEEE and Fellow of Higher Education Academy (FHEA). He is the General Chair of the 27th IEEE ICECS 2020, and serves on the organizing committee of several conferences.